

1 **Title:**
2 **Modeling the Global Emission, Transport and Deposition of Trace Elements Associated with Mineral Dust**
3 **Authors:**
4 Y. Zhang [yan_zhang@fudan.edu.cn]
5 N. Mahowald [mahowald@cornell.edu]
6 R. A. Scanza [ras486@cornell.edu]
7 E. Journet [emilie.journet@lisa.u-pec.fr]
8 K. Desboeufs [karine.desboeufs@lisa.u-pec.fr]
9 S. Albani [s.albani@cornell.edu]
10 J. F. Kok [jfkok@ucla.edu]
11 G. Zhuang [gzhuang@fudan.edu.cn]
12 Y. Chen [yingchen@fudan.edu.cn]
13 D. D. Cohen [dcz@ansto.gov.au]
14 A. Paytan [apaytan@ucsc.edu]
15 M. D. Patey [mpatey@gmail.com]
16 E. P. Achterberg [eachterberg@geomar.de]
17 J. P. Engelbrecht [Johann.Engelbrecht@dri.edu]
18 K. W. Fomba [fomba@tropos.de]
19

20
21 **Modeling the Global Emission, Transport and Deposition of Trace Elements**
22 **Associated with Mineral Dust**

23 Yan Zhang^{1,2}, Natalie Mahowald², Rachel Scanza², Emilie Journet³, Karine Desboeufs³, Samuel
24 Albani², Jasper F. Kok⁴, Guoshun Zhuang¹, Ying Chen¹, David D. Cohen⁵, Adina Paytan⁶, Matt
25 D. Patey⁷, Eric P. Achterberg^{7,9}, Johann P. Engelbrecht⁸, Khamneh Wadinga Fomba¹⁰

- 26 1. Shanghai Key Laboratory of Atmospheric Particle Pollution and Prevention (LAP³), Department of Environmental
27 Science and Engineering, Fudan University, Shanghai, China
- 28 2. Department of Earth and Atmospheric Science, Cornell University, Ithaca, NY, USA
- 29 3. LISA, UMR CNRS 7583, Université Paris-Est Créteil et Université Paris-Diderot, Créteil, France
- 30 4. Department of Atmospheric and Oceanic Sciences, University of California, Los Angeles, CA, USA
- 31 5. Australian Nuclear Science and Technology Organization, Locked Bag 2001, Kirrawee DC, NSW, 2232, Australia
- 32 6. Earth and Planetary Sciences Department, University of California, Santa Cruz, CA 95064, USA.
- 33 7. Ocean and Earth Science, National Oceanography Centre Southampton, University of Southampton, Southampton
34 SO14 3ZH, UK
- 35 8. Desert Research Institute (DRI), 2215 Raggio Parkway, Reno, Nevada 89512-1095, USA
- 36 9. GEOMAR, Helmholtz Centre for Ocean Research, 24148 Kiel, Germany
- 37 10. Leibniz Institute for Tropospheric Research (TROPOS), 04318 Leipzig, Germany.

38
39 **Abstract** Trace element deposition from desert dust has important impacts on ocean primary
40 productivity, the quantification of which could be useful in determining the magnitude and sign of the
41 biogeochemical feedback on radiative forcing. However, the impact of elemental deposition to remote ocean
42 regions is not well understood and is not currently included in global climate models. In this study, emission
43 inventories for eight elements primarily of soil origin, Mg, P, Ca, Mn, Fe, K, Al, and Si are determined based
44 on a global mineral dataset and a soil dataset. The resulting elemental fractions are used to drive the desert dust
45 model in the Community Earth System Model (CESM) in order to simulate the elemental concentrations of
46 atmospheric dust. Spatial variability of mineral dust elemental fractions is evident on a global scale,
47 particularly for Ca. Simulations of global variations in the Ca/Al ratio, which typically range from around 0.1
48 to 5.0 in soils, are consistent with observations, suggesting that this ratio is a good signature for dust source
49 regions. The simulated variable fractions of chemical elements are sufficiently different; estimates of
50 deposition should include elemental variations, especially for Ca, Al and Fe. The model results have been
51 evaluated with observations of elemental aerosol concentrations from desert regions and dust events in non-
52 dust regions, providing insights into uncertainties in the modeling approach. The ratios between modeled and

53 observed elemental fractions range from 0.7 to 1.6, except for Mg and Mn (3.4 and 3.5, respectively). Using
54 the soil database improves the correspondence of the spatial heterogeneity in the modeling of several
55 elements (Ca, Al and Fe) compared to observations. Total and soluble dust element fluxes to different ocean
56 basins and ice sheet regions have been estimated, based on the model results. Annual inputs of soluble Mg, P,
57 Ca, Mn, Fe and K associated with dust using the mineral dataset are 0.28 Tg, 16.89 Gg, 1.32 Tg, 22.84 Gg,
58 0.068Tg, and 0.15 Tg to global oceans and ice sheets.

59

60 **Key word:** dust; Ca/Al ratio; dust; minerals; atmospheric deposition; global model

61 **1 Introduction**

62 Desert dust aerosols are soil particles suspended in the atmosphere by strong winds, and originate primarily
63 from regions with dry, un-vegetated soils. Desert dust particles are thought to contain several important
64 chemical elements, which can impact the earth system by influencing biogeochemical cycles, in particular,
65 marine primary productivity (Martin et al., 1991; Duce and Tindale, 1991; Herut et al., 1999, 2002, 2005; Okin
66 et al., 2004; Jickells et al., 2005). Iron (Fe) is considered the most important element carried in dust, and low
67 Fe supplies combined with a low dust solubility are thought to limit phytoplankton growth in High Nutrient
68 Low Chlorophyll (HNLC) regions. The HNLC regions feature residual macronutrient (e.g. nitrogen (N) and
69 phosphorus (P)) concentrations, but productivity remains limited by the low supply of Fe (e.g. Martin et
70 al., 1991; Boyd et al., 1998). Further studies have linked Fe to the nitrogen cycle because of high Fe
71 requirements of N fixing organisms (e.g. Capone et al., 1997). While there are internal sedimentary sources of
72 Fe in the ocean, dust deposition is an important source of new Fe to remote regions of the ocean (e.g. Fung et
73 al., 2000, Lam and Bishop, 2008; Moore and Braucher, 2008). Desert dust also contains P, which is a limiting
74 nutrient in some ocean and land regions (e.g. (Mills et al., 2004; Okin et al., 2004; Swap et al., 1992)),
75 especially on longer time scales. In addition, as a dominant constituent of mineral dust, silicon (Si) is an
76 important nutrient for diatoms which are central in ocean productivity (Morel et al., 2003). Other elements
77 released from mineral dust which may be important for ocean biogeochemistry including manganese (Mn) as a
78 biologically essential nutrient and aluminum (Al) as a tracer of atmospheric inputs (e.g. Nozaki, 1997;
79 <http://www.geotraces.org/science/science-plan>).

80 Previous studies have emphasized the importance of measuring elemental composition of dust elements
81 (Kreutz and Sholkovitz, 2000; Cohen et al., 2004; Marino et al., 2004; Marteel et al., 2009), and there are a
82 range of studies highlighting observations of elemental distributions and ecosystem impacts (e.g. Baker et al.,
83 2003; Herut et al., 2002; Buck et al., 2006; Paytan et al., 2009; Chen and Siefert, 2004; Measures and Vink,
84 2000). In-situ observations show evidence of heterogeneities in elemental fractions over arid soil regions
85 (Svensson et al., 2000; Zhang et al., 2003; Shen et al., 2005, 2006; Li et al., 2007). Ratios between elements
86 including Si, Al, Mg, Ca, and in particular Ca/Al ratios have also been used to distinguish dust source regions,

87 for example the Asian desert (Zhang et al., 1996; Sun et al., 2005; Han et al., 2005; Shen et al., 2007) and
88 African deserts (Bergametti et al., 1989; Formenti et al., 2008).

89 Xuan (2005) has simulated the emission inventory of trace elements in the dust source regions of East Asia.
90 However, there has not yet been a study to model the distribution of dust-associated elements on a global scale.
91 Global dust models usually assume a fixed fraction (e.g. normalized to Al) of each element in dust to simulate
92 global dust elemental transport and deposition. For example, Fe is thought to contribute 3.5% and P 0.075% to
93 mineral dust (by mass) (e.g. Luo et al., 2008; Mahowald et al., 2008). Besides spatial variations in elemental
94 compositions, particle size distribution forms another important determinant of elemental abundance in
95 deposited dust. Depending on the particle size distribution, trace elements may remain more or less suspended
96 in the atmosphere and deposited by dry or wet deposition at various distances from desert regions (Seinfeld
97 and Pandis, 1998). There have been very few studies investigating particle size distribution and elemental
98 concentrations in soil and dust by direct measurement (Schütz and Rahn, 1982; Reid et al., 2003; Castillo et al.,
99 2008; Engelbrecht et al., 2009a,b), and even fewer modeling studies have included this. The ability to model
100 the deposition of specific elements associated with dust in global simulations has been hindered by a lack of
101 understanding of the spatial and temporal variability, as well as the particle size distribution associated with
102 different dust sources. As noted by Lawrence and Neff (2009), it seems most appropriate to use a globally
103 averaged value of dust composition to estimate the elemental flux from dust, given the lack of direct
104 measurements of the spatial distribution of elements in dust. However, the use of a global mineral map
105 (Claquin et al., 1999; Nickovic et al. 2012, 2013; Journet et al., 2014) and chemical compositions of minerals
106 (Journet et al., 2008) allows us to simulate global elemental inventories from mineral soils, which could be
107 used in a global dust model.

108 This study aims to introduce a technique to determine a size-fractionated global soil elemental emission
109 inventory based on two different datasets, a global soil dataset and a mineralogical dataset. A companion paper
110 evaluates the ability of the model to simulate mineralogy and the impact on radiation (Scanza et al., 2015). The
111 elemental emission dataset estimated for Mg, P, Ca, Fe, Mn, K Al, and Si was used as an input to a model
112 simulation of the global dust cycle to present the elemental distributions, which were compared against
113 available observations of concentration and deposition to different ocean regions.. Our goal is to assess the
114 variability of elemental fractions in atmospheric and deposited dust, and to investigate whether the elemental
115 emission dataset can adequately predict this variability. This study focuses on desert dust particles, and thus
116 disregards other potentially important sources of the elements such as combustion processes (e.g. Guieu et al.,
117 2005; Luo et al., 2008; Mahowald et al., 2008). We focus on total elemental concentrations, but discuss two
118 methodologies for soluble metal distributions from soil emissions. We also do not consider any atmospheric
119 processing, which is likely to be important for some chemical components (e.g. Mahowald et al., 2005; Baker
120 and Croot, 2010).

121

122 **2 Materials and Methods**

123 2.1 Soil and mineral datasets

124 The soil map of the world used in this study comes from the Food and Agriculture Organization (FAO) of
125 the United Nations soils dataset, and includes 136 soil units [FAO-United Nations Educational, Scientific, and
126 Cultural Organization (FAO-UNESCO, 1995) at a 5-minute resolution. The global dataset of soil clay and silt
127 data are used in this study. Following [Claquin et al. \(1999\)](#) and [Nickovic et al. \(2012\)](#), the illite, hematite,
128 kaolinite, smectite, quartz, feldspars, calcite and gypsum contents are specified for different clay and silt soil
129 types, and the global mineral distribution is presented in [Scanza et al \(2015\)](#). Some minerals found in dust such
130 as dolomite were not considered by [Claquin et al. \(1999\)](#) and [Nickovic et al. \(2012\)](#) and have also been
131 disregarded in this study due to the lack of data on their distribution.

132 The elemental compositions of hematite and aluminosilicate minerals used in this study are taken from
133 previous works ([Journet et al. \(2008\)](#) and unpublished data provided by E. Journet, 2012) and were obtained by
134 X-ray fluorescence spectrometry (XRF) (Table 1a). Most of minerals used by [Journet et al. \(2008\)](#) are
135 reference materials from the Society's Source Clays Repository, i.e. hematite, illite, kaolinite, montmorillonite.
136 The elemental compositions obtained by XRF are in the range of published values for these reference materials
137 (e.g. [Mermut and Cano, 2001](#); [Gold et al., 1983](#)), validating the obtained composition for the unreferenced
138 materials. Moreover, the purity of all minerals samples is estimated by X-Ray diffraction. Note that the
139 mineralogical maps used in this study do not distinguish feldspar and smectite subtypes. For feldspars, the
140 elemental composition is mostly averaged based on 2 subtype minerals: orthoclase (potassic feldspar) and
141 oligoclase (sodium-calcium feldspar). For smectites, the montmorillonite subtype is the most commonly
142 identified smectite in desert dust, particularly for Saharan dust e.g. [Goudie and Middleton, 2006](#)). The
143 chemical composition of montmorillonite is used in this study as an analog for smectite. For calcite, gypsum,
144 and quartz, the natural minerals could contain substitutions or impurities from clays, which are
145 variable depending on origin, formation, contamination, etc. of minerals. Because regional silt samples were
146 not available for spectroscopy, we use the theoretical composition of elements in calcite, gypsum and quartz
147 (Table 1a). The mass fraction of Ca in calcite (CaCO_3) and gypsum ($\text{CaSO}_4 \cdot 2\text{H}_2\text{O}$) are taken as 40% and
148 23.3%, respectively. A mass fraction of 46.7% Si is used for pure quartz (SiO_2).

149 Following the total element calculation, soluble elemental fractions are estimated based on soluble elemental
150 contents of minerals at pH=2 reported by [Journet et al \(2008\)](#) for hematite and the aluminosilicates, and is
151 listed in Table 1b. The fractional solubility of Ca in calcite and gypsum used is 7% and 0.56%, respectively,
152 and that of Si in quartz was 0.0003% based on individual solubility product (K_{sp}) at pH=2 ([Petrucci et al.,](#)
153 [2001](#)). Here the mineral dependent method used to calculate soluble elements is defined as Method 1 (Sol-1).
154 To present uncertainties, another approach (Method 2, defined as Sol-2) is introduced as a reference. It is based
155 on the extractable elemental fractions of in-situ 20 μm sieved soil samples reported by [Sillanpaa \(1982\)](#) (Table
156 S1) and is combined with an FAO soil dataset to get a global soluble elemental inventory independent of soil
157 minerals. It is noted that there is no detailed size distribution for soil samples in Sol-2. Thus, the fractions of
158 soluble elements in clay and silt are assumed to be equal to that of the bulk soils themselves.

159 Table S1 Averaged macronutrient contents (%) of soils classified by FAO/Unesco soil units *

160 One drawback of our approach is that we disregard the large variability of soils included within each defined
161 “soil type”. The range of minerals within each soil type is large (e.g. Claquin et al., 1999), and the range of
162 elemental concentrations in each mineral is also large (Journet et al., 2008). The resolution of our model is
163 such that despite the actual heterogeneity of soils at a particular location, we prescribe an average at each
164 gridbox which tends to reduce the variability in elemental composition in the mineral dust in the atmosphere.
165 This is likely to be the largest source of uncertainty in our approach.

166 **Table 1 (a) Generalized mineral compositions (%) applied in this study ;(b) Elemental solubility as a percentage of**
167 **the element contained in the minerals (%)**

168 **Table 2 Emission rates (Tg/yr) and percentages of elements over desert regions (%)**

169

170 2.2 Numerical Model description

171 Community Earth System Model version 1.0.3 (CESM1.0.3) is coordinated by the National Center for
172 Atmospheric Research (NCAR), and has been used to simulate elemental dust emission, transport and
173 deposition in this study. The bulk mineral aerosol in the Community Atmosphere Model version 4 (CAM4)
174 was adapted to include eight trace elements within total dust (Scanza et al., 2015). In this model simulation, the
175 physical scheme CAM4 is driven by the meteorological dataset MERRA, and is simulated spatially at 1.9×2.5
176 degree resolution for the years 2000-2010. The soil erodibility map used by the dust model has been spatially
177 tuned (Albani et al., 2014). There are four size classes of dust particles used in the dust emission module in the
178 bulk scheme with particle diameters of 0.1-1.0, 1.0-2.5, 2.5-5.0 and 5.0-10.0 μm . The sub-bin size distribution
179 is assumed to follow a log-normal distribution with a mass median diameter of 3.5 μm (Mahowald et al., 2006)
180 and a geometric standard deviation of 2.0 μm (Zender et al., 2003). Combining these log-normal parameters
181 with the brittle fragmentation theory of dust emission (Kok, 2011) yields each bin’s partitioning of dust aerosol
182 mass between the soil’s clay and silt size fractions (see Table B3 and Scanza et al., 2015). The elements in the
183 dust undergo three-dimensional transport individually in each of the different size bins, identically to bulk dust
184 in the original model. Elemental atmospheric mixing ratios, and wet and dry deposition are updated at each
185 model time step based on actual elemental fields and the corresponding tendencies.

186 There has been considerable work on improving advection algorithms in atmospheric models, and here we
187 use the finite volume advection algorithm as part of the CAM (Lin and Rood, 1997). While no advection
188 scheme is perfectly mass conserving, monotonic, shape preserving and computationally efficient, this scheme
189 does a good job of balancing these multiple goals and maintaining strong gradients required in modeling
190 atmospheric constituents (e.g. Rasch et al., 2006). By splitting the dust into its different mineral elements, we
191 may add in additional numerical errors, because the advection will not conserve the fraction of elements within
192 dust aerosols due to small numerical errors. For the discussion of the ratios of elements, it would be better to
193 advect the minerals themselves, and evaluate the ratio of elements later, since this would better conserve the
194 ratios. Studies focused on elemental ratios and their distribution in ocean models have suggested there is a
195 relatively small uncertainties associated with these types of numerical errors (e.g. Christian, 2007), and

196 compared with the errors in the source distribution of the minerals, errors from advection are likely to be small
197 and are neglected here.

198 **Table S2. The fraction of dust aerosol mass contributed by the soil clay and silt fractions for each of the 4 particle size**
199 **bins for the bulk scheme in CAM4.**

200

2012.3 Observational data

202 An element dataset of ground based aerosol measurements at 17 sites (Table B3) is used to evaluate the
203 elemental dust simulation (Sun et al., 2004a,b; Wang et al., 2010; Chen et al., 2008; Engelbrecht et al., 2009;
204 Carpenter et al., 2010; Cohen et al., 2011; Guo et al., 2014; Formenti et al., 2008; Desboeufs et al., 2010). The
205 sites are close to major dust-producing regions (Figure 1), including 10 Asian sites (Central Asia: Hetian,
206 Tazhong; East Asia: Yulin, Duolun, Shengshi; South Asia: Hanoi, and Manila; Middle East: Balad, Baghdad,
207 Taji), 5 African sites (West Africa: Cape Verde Atmospheric Observatory (CVAO); East Africa: Eilat; North
208 Africa: Tamanrasset, Banizoumbou, and Douz), and 2 Australian sites (Muswellbrook, Richmond). Generally,
209 these field aerosol samples (Total Suspended Particulates (TSP), PM₁₀, PM_{2.5}) have 1-3 day collection periods
210 during the period 2001-2010, and were chemically analyzed for elemental composition. No observational
211 aerosol mass concentrations at the Cape Verde station could be used in this study. At this site, the particulate
212 matter (PM) concentrations are estimated by assuming an Al to total dust mass ratio of 0.0804. In order to be
213 certain that only desert dust elements are compared with the model results, only data collected during dust
214 storm seasons are selected. Measurement sites from which data are taken are listed in Table B3, which includes
215 related methodological details.

216 In addition, the dataset of dust deposition at more than 100 sites worldwide is used to evaluate modeled dust
217 deposition fluxes (Albani et al., 2014).

218 **Fig.1. Observational sites** (S1-Hetian, China; S2-Tazhong, China; S3-Yu Lin, China; S4-Duolun, China; S5-
219 Shengsi, China; S6-Hanoi, Vietnam; S7-Manila, Philippines; S8- Balad, Iraq; S9-Balad, Iraq; S10-Taji, Iraq; S11-
220 Eilat; S12-Cape Verde Atmospheric Observatory (CVAO); S13-Muswellbrook, Australia; S14-Richmond, Australia;
221 S15-Tamanrasset, Algeria; S16-Banizoumbou, Niger; S17-Douz, Tunisia) **and dust-producing regions** (WAsia:
222 West Asia; NC-As: North Central Asia; CAsia: Central Asia; SC-As: South Central Asia; EAsia:East Asia; WN-
223 Af:North West Africa; EN-Af: North East Africa; S-NAf: Southern North Africa; SAf: Southern Africa; MNWAm:
224 Middle North West America; SNWAm: Southern North West America; SAM1: Northern South America; SAM2:
225 Southern South America; WAus: West Australia; EAus: East Australia)

226 **Table S3. Locations of 17 sampling sites**

227 3 Results and Discussion

228 3.1 Fractions of element in arid soil regions

229 The global distributions of the elements Mg, P, Ca, Mn, Fe, K, Al, and Si in bulk soils as mass percentages
230 in soils are presented in Fig. 2.

231 3.1.1 Global mapping of soil associated elements

232 Fractions of elements in soils vary between mineralogical clay and silt fractions. Spatial variability of soil
233 chemistry is seen on a global scale (Fig.2). A large range of variability for some elements within one given
234 source region is observed (e.g. Ca, Fe, Mn, Al). The most extreme variability is observed for Ca in soil silt,
235 which varied from 0.5 to 34.3%, and is much higher in West and Central Asia, South Africa and Northern
236 South America than in other parts in the world. This is ascribed to the presence of feldspar and gypsum, both
237 being important source minerals for Ca in these regions. In Central and East Asia, the Ca content increased
238 from east to west, showing a similar spatial trend to that reported by Xuan et al. (2005). A south to north
239 gradient of Ca content was also observed in the Sahara following the carbonate distribution of soils (Kandler et
240 al., 2007; Formenti et al., 2011). In southern North Africa, South Africa and the Western Australia, clay soil
241 and fine dust emissions have higher Al and P concentrations than elsewhere. In Eastern Australia, Patagonia,
242 and the northern South Africa, the Fe content of soils is also higher than in other regions. Due to their high
243 content of quartz, soils generally have 25-40% Si. These elemental distributions are in agreement with other
244 published data for Fe, as they are derived from similar regions (e.g. Claquin, 1999; Hand, 2004).

245 **Fig.2 Global elemental distributions (in mass percentage) in a1: Clay Mg, a2: Clay P, a3: Clay Ca, a4: Clay Mn, a5: Clay**
246 **Fe, a6: Clay K, a7:, Clay Al, a8: Clay Si; b1: Silt Mg, b2: Silt P, b3: Silt Ca, b4: Silt Mn, b5: Silt Fe, b6: Silt K, b7: Silt Al,**
247 **b8: Silt Si.**

248 3.1.2 Elemental composition of soils and airborne dust

249 Trace elements in soils show different associations with particle size patterns depending on the size
250 distribution of soil minerals. For example, Mg, P, Fe, Mn, and Al are dominant in the clay size fraction (< 2
251 μm) (Fig. 3b). Fractions of Al and Fe reach 11.7% and 3.1% in clay fractions of soils, while only 2.8% and 1.2%
252 in silt fractions of soils, respectively. However, Ca and Si show a slight enrichment in coarser soil fractions. Ca
253 comprises 2.6% of soils in the clay fraction but 3.6% in the soil silt fractions. This is consistent with the size
254 distribution of Ca and Fe-rich individual particle groupings measured in Saharan dust (Reid et al., 2003). K has
255 nearly equal distributions in clay and silt fractions of soils. Taking the fractions of elements in soils as inputs,
256 the fractions of elements in dust emission can be predicted. Our classification of soil particles into four aerosol
257 sizes (Table B2) provides heterogeneity in elements across sizes, but allows for a mixing across soil sizes,
258 reducing the differences among size fractions. For example, the percentage of Fe remains unchanged from clay
259 soil to fine mode dust emission, but changes substantially from silt soil (1.2%) to coarse mode dust (2.2% in
260 Bin 3). A similar pattern appears for the other elements, and the differences between elemental percentages
261 in the soils are reduced when dust emissions are considered (Fig. 3a vs. 3b).

262 **Fig.3 Global mean elemental percentages in (a) four-bin dust emission and (b) clay and silt fractions of soils (Bin1-4 refer to**
263 **particle range listed in Table S2, clay refer to <2 μm , silt refer to > 2 μm)**

264 3.1.3 Elemental dust emissions over desert regions

265 Annual elemental dust emissions over 15 dust-producing regions (shown in Fig.1) are determined (Table 2).

266 The annual average of total global dust emission is estimated to be 1582 Tg based on 2001-2010 simulations,
267 and is within the wide range (514 to 5999 Tg/yr) as reported by previous studies (e.g. Textor et al., 2006,
268 2007; Prospero et al., 2010; Huneus et al., 2011). Africa and Asia account for 68% and 31% of the global
269 emissions, respectively. Correspondingly, trace element emissions are dominant from African desert regions,
270 with percentages ranging between 65%-70%. Specifically, Al emission from Africa account for 70% of global
271 Al emissions, of which 64% originated from the Western Sahara. For Asian desert regions, elemental dust
272 account for 29-34% of the global total amount, with Ca being the strongest contributor (34%) to global Ca
273 emissions. The percentage of Fe is similar to Al in the total dust emissions with 67% and 32% of Fe from
274 Africa and Asia, respectively. The maximum % element for Ca at 5% was in dust emission from West Asia,
275 being more than 4 times higher than Southern North Africa (1.2%). However, the fraction of Al and Si is
276 largest in dust emission from Southern North Africa, with values of 9.0% and 31%, respectively. The fractions
277 of Fe and P are 2.8%, and 0.08% in Australia, which is higher than that in other source regions. The simulated
278 elemental fractions in dust suggest that differentiating elements in soils between global source areas is
279 necessary and meaningful.

280 **Table 2 Emission rates (Tg/yr) and elemental composition of dust over desert regions (%)**

281

282 **3.2 Spatial and seasonal distribution in fractions of elements in atmospheric and deposited** 283 **dust**

284 **3.2.1 Elemental fractions in global atmospheric dust and deposited dust**

285 The modeled fractions of different elements in atmospheric dust have substantial spacial variability (Fig. 4). Fe
286 content is greater than 2% for most regions, with a global mean of 2.7% in atmospheric dust. The maximum
287 contributions of Fe, Al, P and Mn fractions are observed in the tropical Pacific region with values greater than
288 3%, 10%, 0.08%, and 0.02%, respectively. For Ca, Si and K, a higher fraction is evident in terrestrial
289 environments. There are obvious land-ocean gradients existing in the distributions of elemental fractions, with
290 higher Ca and Si fractions in terrestrial regions and higher P, Fe, and Al fractions in oceanic areas, likely due
291 to their differences in particle size distribution (Fig. 3). There are very similar spatial patterns and magnitudes
292 shown for the elemental fractions in deposited dust compared with those in atmospheric dust for each element
293 (Fig. S1, Fig. 5). Higher fractions of Ca and Si in deposited dust is observed in regions close to desert dust
294 sources where the two elements occur in the coarser size fractions. Conversely, lower Mg, P, Mn, Fe and Al
295 contents are found in dust deposits close to source regions but higher contents are found over oceans, which is
296 consistent with the clay soil fraction dominating the finer particle size fractions. The importance of relative
297 location of the source compared to the deposition to the elemental ratio adds complexity in applying simple
298 percentages to dust deposition to obtain elemental deposition amounts.

299

300 Fig.4 Percentages of elements in dust concentration (mass %) : a. Mg, b. P, c. Ca, d. Mn, e. Fe, f. K, g. Al, h. Si.
301 Elemental % shown here are calculated using the annual mean element concentration divided by the annual mean dust
302 concentration.

303 Fig.S1 Percentages of elements in deposited dust (%) :a. Mg, b. P, c. Ca, d. Mn, e. Fe, f. K, g. Al, h. Si. Elemental
304 annual mean % are calculated using the annual mean emission of each element divided by the annual mean emission of
305 dust.

306 Fig.5 Ratio of mass fractions of elements in dust deposition to that in atmospheric dust : a. Mg, b. P, c. Ca, d. Mn, e. Fe, f.
307 K, g. Al, h. Si. Elemental ratios shown here are calculated using the annual mean element deposition divided by the
308 annual mean dust deposition.

309

310 3.2.2 Seasonal variability of elemental fractions

311 As described above, the fractions of elements in dust fluctuate temporally and spatially on a global scale. There
312 are seasonal variations in dust emissions from various desert regions showing different emission patterns
313 (Fig.S2). The peak periods for dust emissions for various desert regions are consistent with those found by
314 Werner et al., (2002) (Figure S2). Combining the seasonal cycles in atmospheric dust production with the
315 element distributions in desert regions, the elemental fractions show large monthly variability but small inter-
316 annual variability during 2001-2010 (Fig. A3). Ca and Al have clear seasonal cycles, with Ca having the
317 largest monthly variability with peak concentrations in the between July and September. This is ascribed to the
318 higher Ca content of dust originating in West Asia, Central Asia and Southern Africa, regions that provide
319 large global dust emissions in this period (JJAS).. For the other elements, the peak concentrations usually
320 occurred between March and May (MAM) or November through January (NDJ), corresponding to the periods
321 when global dust emissions reach a maximum.

322 We modeled the seasonal variability of these elemental fractions. Elemental percentages are calculated using
323 the climatological monthly mean emission of each element divided by the climatological monthly mean
324 emission of dust. An index describing monthly variability is calculated by:
325

$$326 \text{ Monthly variability (\%)} = \frac{SD \text{ of mean fraction}_{month}}{\text{Mean fraction}_{month}} \times 100 \quad (\text{Eq. 1})$$

326

327 Twelve monthly mean fractions are averaged from the ten year simulation, with the corresponding standard
328 deviations (SDs).. Finally, the percentages (Eq.1) of the standard deviation in the monthly means is derived to
329 describe the variability in elemental fractions of atmospheric dust and deposited dust (Fig. 6 and 7).

330 The monthly mean variation is greatest for Ca, reaching more than 30% variability in some regions. The
331 temporal variability of elemental percentages in deposited dust tended to be larger than those in atmospheric
332 dust and show a greater spatial gradient from land to sea. That is similar to the trend of the elemental fractions
333 in atmospheric and deposited dust (section 3.2.1) since the temporal variation is originally induced by the

334 spatially variable elemental fraction. In the South Indian Ocean and the South Atlantic Ocean, the monthly
335 variability is even higher and is attributed to the combined effect of variability in dust emissions,
336 spatial elemental concentration, and dust transport patterns.

337

338 **Fig.S2 Monthly dust emission (kg/m²/s) over 15 dust-producing regions (WAsia: West Asia; NC-As:North Central Asia;
339 CAsia:Central Asia; SC-As: South Central Asia; EAsia:East Asia; WN-Af:North West Africa; EN-Af: North East Africa;
340 S-Naf: Southern North Africa; SAF: Southern Africa; MWNA: Middle North West America; SWNA: Southern North
341 West America; SAM1: Northern South America; SAM2: Southern South America; WAus: West Australia; EAus: East
342 Australia)**

343 **Fig.S3 Seasonal cycle of global mean elemental percentages (%) in atmospheric dust from 2001 to 2010. Elemental % are
344 calculated using the climatological monthly mean emission of each element divided by the climatological monthly mean
345 emission of dust.**

346

347 **Fig.6 Ten-year monthly variability in mean of elemental percentages in atmospheric dust (mass %) : a. Mg, b. P, c. Ca, d.
348 Mn, e. Fe, f. K, g. Al, h. Si. Elemental monthly mean % are calculated using the monthly mean emission of each element
349 divided by the monthly mean emission of dust.**

350 **Fig.7 Ten-year monthly variability in mean of elemental percentages in dust deposition (mass %):a. Mg, b. P, c. Ca, d.
351 Mn, e. Fe, f. K, g. Al, h. Si. Elemental monthly mean % are calculated using the monthly mean emission of each element
352 divided by the monthly mean emission of dust.**

353

354 **3.3 Spatial Ca/Al distribution in soils and dust plumes**

355 Of specific interest is the Ca/Al ratio in soil, atmospheric dust and deposited dust as this ratio may be
356 indicative of specific source regions (Fig. 8). Of all considered ratios, the Ca/Al ratio in soils show the greatest
357 variability in relation to the relevant desert region (e.g. [Formenti et al. \(2011\)](#)). The Ca/Al ratio ranges mainly
358 between 0.1-1 in clay fractions of soils and 0.5-5.0 in silt fractions of soils (Fig. 8a,b). The maximum Ca/Al
359 ratios reaches 160 times the global mean Ca/Al ratio of 1.96 in the silt fraction of soils (Fig. 8b), much higher
360 than those of other ratios such as Fe, K, and Mn to Al. Asian desert soils have higher Ca/Al ratios, with values
361 greater than 5 in West Asia and Central Asia. The Ca/Al ratio in dust emissions from Central Asia (1.0-1.6) are
362 higher than in East Asia (~0.5), which is close to Ca/Al ratios (1.0-1.7) derived from source profiles of Asian
363 dust ([Zhang et al., 1997](#); [Zhang et al., 2003](#)), and also match the observed Ca/Al ratios (0.7-1.3) during Asian
364 dust events ([Sun et al., 2004a,b](#); [Shen et al., 2007](#)). In addition, the Ca/Al ratio in dust emissions in North
365 Africa are below 0.5, confirming the application of the Ca/Al ratio of 0.3 (or 3.8 with Al/Ca) as an indicator of
366 North African dust transport to the eastern United States ([Perry et al., 1997](#)). Ambient PM_{2.5} dust measured on
367 the Canary Islands suggests a different ratio (Ca/Al = 1.004) ([Engelbrecht et al., 2014](#)). However, this ratio
368 could be larger for PM₁₀ or TSP. The high Ca/Al ratio (4.0-10.0) in a range of desert soils in some regions
369 including South Africa, yields a Ca/Al ratios in dust emissions of 1.0, being much larger than those from North
370 Africa. The modeled spatial pattern of Ca/Al ratio in dust emissions from Asia and northwest Africa is
371 consistent with the currently available dust pattern compiled by [Formenti et al. \(2011\)](#), but shows relatively
372 lower values for the Central Asian desert region.

373 Despite experiencing mixing of airborne dust from various source regions and as a result of dust processing
374 during transport, the Ca/Al ratios still show spatial variations in global atmospheric dust and deposited dust.

375 Relative to the Ca/Al ratio in source regions (Fig. 8a,b), the Ca/Al ratio in atmospheric dust over most of

376 terrestrial Asia ranges between 0.5-0.8, with a maximum of 1.8. This is due to the spatial variability of Ca/Al
377 ratio in dust emissions (Fig. 9a) and despite the preferential gravitational settling during transport of silt
378 fraction which represents the highest Ca/Al variability. The variability in Ca/Al ratio in dust deposited into
379 oceans and onto ice sheets are also shown in Fig. 9b. Near West Asia and Western Sahara, higher Ca/Al ratios
380 are noted and the North Indian ocean and Mediterranean sea have a Ca/Al ratio above 0.65 in deposited dust.
381 As the combined downwind region of central Asia and East Asia, the North Pacific has a Ca/Al ratio around
382 0.5. The Ca/Al ratio in dust deposited over the Atlantic ranges between 0.3-0.4 due to the influence of southern
383 North Africa desert region and East Sahara desert both with low ratios of Ca/Al. Since the soil dataset has a
384 high spatial resolution of 5 arc minutes (Fig. 8a,b), there is opportunity to increase the model grid resolution
385 ($1.9 \times 2.5^\circ$ in this study) to a finer resolution. It is expected that Ca/Al ratio will show more spatial
386 heterogeneity when a finer model resolution is used. We conclude that the Ca/Al ratio can be used to identify
387 different source areas and the model can be used to support the observations.

388

389 **Fig.8 Ca/Al in Soil and ten year averaged Ca/Al ratio in dust emission, concentration and deposition. Top two (a,b) refer**
390 **to ratio in clay and silt desert soil, middle one (c) refer to ratio in dust emission, and bottom two (d,e) refer to ratio in dust**
391 **concentration and deposition. Elemental annual mean % are calculated using the annual mean emission of each element**
392 **divided by the annual mean emission of dust.**

393 **Fig.9 Ten year averaged Ca/Al ratio in (a) dust emission of source regions and (b) dust deposition into various ocean**
394 **basins and glaciers. Elemental ratios are calculated using the annual mean emission of Ca divided by the annual mean**
395 **emission of Al.**

396 **3.4 Model evaluation with observational data**

397 The averaged modeled fractions of elements in atmospheric dust at each site for the periods for which
398 observations are available are comparable with observations for most of the sites (Fig. 10a,b). It is clear most
399 scatter values of model and observations are in the range of 2:1 and 1:2 line for most elements in TSP
400 except for Mg, Mn and Si. It shows the emission inventories based on mineralogy and elemental
401 compositions are generally consistent with the available data. A large variability in the percentage of different
402 elements is observed at the 17 observational sites for most elements, especially for Ca (Fig. 10). The fraction
403 of Fe in the fine mode particle ($PM_{2.5}$) is closer to the observational data than the TSP Fe fraction, implying that
404 Fe in the clay soils is more accurate than that for silt. Since there are only a few reported observations of Si,
405 this element is particularly difficult to verify. Based on averaged elemental fractions in TSP at 13 sites, the
406 correlation coefficients (R) between modeled and observed fractions range widely (Table 3). Ca and Al had the
407 highest correlations (0.75 and 0.72, respectively). However, the correlation coefficients for P, Mn and K were
408 negative. For Fe, if we neglect the 3 sites in North Africa, the correlation coefficient increases from 0.29 to
409 0.50; in this area, the observational Fe fractions in TSP are high whereas the modeled ones are low (Fig.
410 10.a,5). The modeled elemental fractions in TSP are close to the observed data, with most ratios ranging
411 between 0.7 and 1.6 (Table3).

412 For this comparison (above), we calculate the elemental fractions and average the fractions temporally for each
413 site and compare to observations, but alternatively, we could average the elemental concentrations and divide
414 by the elemental dust concentrations instead, and this will make a difference in our interpretations. For
415 example, taking site 2-Tazhong, the averaged fraction is 3.5% when we calculate the fractions of iron firstly
416 and average those temporally. However, when we calculate the averaged iron mass and dust mass separately,
417 their ratio is 2.3%. For site3-Yulin, the ratio is 3.6% and 3.1% for the first method and second method,
418 respectively. This difference maybe due to dust storm events. For this comparison, we use the first method, as
419 we think it is more suitable for our goal of simulating the percentage of each element correctly.

420 The averaged fractions of Mg and Mn in dust are underestimated by the model at all observational sites. It
421 should be noted that there are some uncertainties when comparing elemental fractions. When the elemental
422 concentration is divided by particle mass concentration to obtain the elemental fraction, the errors are
423 amplified due to error propagation associated with the combination of the error on the particle mass and that of
424 the element concentrations. Even though the available observational data are chosen from source sites or dust
425 events in non-source regions, the contribution from other sources could be important, especially for fine mode
426 particles. The modeled fraction of Mn and Al in fine particles show a larger inconsistency than that those in
427 TSP when compared with observations. Some of the discrepancies may be because the model only includes
428 particles up to 10 μm in diameter, while the observations include larger particle fractions in TSPs. In South
429 Asia, the elemental fractions in dust with the exception of Mn, are always much lower than at another sites,
430 perhaps due to anthropogenic contributions to elemental particulate matter concentrations. In particular, many

431 metals in insoluble forms in dust particles could be from other sources such as the refractories and steel
432 industries, construction, biomass burning or volcanic emissions (Castillo et al., 2008;Gaudichet et al., 1995;
433 Hinkley et al., 1999; Paris et al., 2010).

434 The daily elemental fractions across all times and sites where there is data show that while the mean of the
435 model was similar to the mean of the observations, there are some systematic differences (Figure 11a,b). The
436 modeled elemental fractions are not as variable as the observations. This could be due to several issues. First
437 there is a greater variability in the soil mineralogy and elemental composition of minerals than those included
438 in the model (we only include the average values). Secondly, the dust model could introduce systematic errors
439 (through advection, although this is likely to be small, as discussed in the methods section 2.1), or there could
440 be some unaccounted anthropogenic particulate sources, modifying the dust aerosol. Also inconsistencies in
441 the collection methods and differences in aerosol sampling periods and times could yield the observed
442 variations in elements as concluded by Lawrence and Neff (2009).

443 However, the ranges of the modeled fractions of P, Ca, Fe, K and Al are close to the dominant range of the
444 observational fractions (Fig. 11a,b). The fractions of elements in dust measured are reported to be 0.5%-2.3%
445 for Mg, 0.065-0.2% for P, 1.0-10.2% for Ca, 0.028%-0.124% for Mn, 1.3%-7.8% for Fe, 1.2%-4.6% for K,
446 3.7-12.7% for Al, and 22.4%-35.7% for Si (Wilke et al. ,1984; Reheis and Kihl,1995; Stoorvogel et al., 1997;
447 Zhang et al.,1998; Yadav and Rajamani,2004; Goudie and Middleton, 2006; Moreno et al., 2006; Jeong, 2008;
448 Lawrence and Neff, 2009; Formenti et al., 2008; Desboeufs et al., 2010). The modeled elemental fraction in
449 dust for P, Ca, Fe, K, Al and Si were similar to observations. However, the modeled fractions of Mg and Mn
450 are lower (3.4 times and 3.5 times, respectively (Table 3)) than the observed ones for samples used in this
451 study or of the above cited results. Underestimation of Mg and Mn could be due to a deficiency of minerals
452 containing high concentrations of Mg and Mn in our model, as dolomite ($MgCO_3$) or palygorskyte
453 ($(Mg,Al)_2Si_4O_{10}(OH)\cdot 4(H_2O)$) are often identified in dust particles for Mg (e.g. Diaz-Hernandes et al., 2011;
454 Kalderon et al., 2009). Moreover, it is known that the chemical composition of minerals could be variable
455 according to the regional origin of minerals and possible impurities. For example, the Mg content in calcite
456 ranges from 0% to 2.7% in the natural environment (Titschack et al., 2011). But in this study, the assumed
457 fraction of Mg in calcite is zero because we took calcite as a pure mineral (see Table 1). So the
458 underestimation of Mg in dust could be a propagation of errors in previous compositions in minerals
459 considered in this study.

460

461 **Fig.10 Comparison of observed and modeled mean fractions of elements at each site for total suspended particulates (TSP).**
462 **(1-Hetian, China; 2-Tazhong, China; 3-Yu Lin, China; 4-Duolun, China; 5-Shengsi, China; 6-Hanoi, Vietnam; 7-Marnila,**
463 **Philippines; 8- Balad, Iraq; 9-Baghdad, Iraq; 10-Taji,Iraq; 11-Eilat; 12-Cape Verde Island; 13-Muswellbrook, Australia;**
464 **14-Richmond, Australia, 15-Tamanrasset, Algeria; 16-Banizoumbou, Niger; 17-Douz, Tunisia).** Here we calculate the
465 elemental fractions and average the fractions temporally for each site and compare to observations.

466
467

468 **Fig.11 Mean and quartile modeled and observational fractions of elements in (a) TSP and (b) PM_{2.5} for all sites**
469 **together, the box line presents 25%, 50% and 75%, individually.** Here we calculate the elemental fractions and
470 average the fractions temporally for each site and compare to observations.
471

472

473

474 **Table 3 Comparison of modeled and observed fractions of elements in TSP and tuning ratio based on 14-site**
475 **measurements**

476

477 For reference we show the comparison of the modeled dust deposition versus observed deposition (Fig. 12).
478 The modeled dust deposition flux agrees well with observations. The correlation coefficient between modeled
479 and observed dust deposition is 0.86. The median of model to observation ratio is 1.15. Overall the model has
480 been tuned to represent dust deposition, concentration and Aerosol Optical Depth (AOD) (Albani, et al., 2014),
481 however the model has difficulty matching both deposition and concentration observations, similar to other
482 models (Huneeus et al., 2011), suggesting more work on dust emission, transport and deposition processes is
483 needed.

484 **Fig.12 (a) Observational and (b) modeled dust deposition (g/m³/year). The scale is the same for both panels. (c) A scatter**
485 **plot shows the comparison between the model and observations. The correlation coefficient between observations and**
486 **model results reach 0.86.**

487 **3.5 Deposition of total and soluble dust elements over the ocean, land and ice sheets**

488 Comparisons between observations and the model simulations presented here suggest some bias in the model
489 results (Figure 11, Table 3); subsequently the model deposition values are adjusted to better match observed
490 measurements by the tuning ratios (Table 3; Figure 13).. Of course, improving our elemental estimates in the
491 source region would be preferred in future studies. From the observations, we have found a wide range in
492 fractions of elements at individual sites and at the sites together; the ratio of the maximum and minimum in
493 measured fractions could reach more than 700 for element K, and more than 200 for Ca and Mn. Because of
494 the limited observations, we use a global tuning factor, based on the median elemental percentage, and contrast
495 this result with our default modeling approach (Table 3). It is noted that both the median of observed (3.10 %) and modeled (2.9 %) Fe was lower than 3.5%, which was thought to be the fraction of Fe in dust (e.g. Luo et al., 2008; Mahowald et al., 2008).

498 This study suggests significant variability in the elemental fractions in dust deposition (Figure 13, Table 4),
499 and showed that the assumption that the fixed composition of dust being deposited over oceans is unlikely to
500 be correct. Consistent with Mahowald et al. (2008), most dust deposition occurred downwind of dust
501 generating regions bordering the North Atlantic, North Pacific and North Indian Ocean. The Greenland ice
502 sheet accounted for the dominant part of elemental deposition to ice sheets regions, which is equal to the total
503 amount of elements deposited in the whole of the South Atlantic Ocean. Fe and P are key elements in the
504 marine ecosystem, with 6.3 Tg Fe and 184 Gg P added annually to all oceans and ice sheets (Table 5).

505 **Table 4 Fractions (%) of elements in dust deposition into different ocean basins and ice sheets***

506 Also, the amounts of soluble dust element deposition are determined over different regions (see Section 2.1)
507 (Figure 14). No atmospheric processing of natural dust or other sources of particles (e.g. anthropogenic sources)
508 is included in this simulation. To better understand the uncertainties of soluble element deposition, estimates
509 from two methods are used (Section 2.1) in simulating soluble elemental emission, transport and deposition.
510 Fractional solubility of elements could not be estimated due to the lack of total element data from Method 2
511 (Sillanpaa (1982)). Spatial variations in fractional solubility of elements are identified by Sol-1 (mineral
512 method) (Fig.14). Fractional solubility of Ca increases with distance from source regions because its solubility
513 is higher in clay than in silt (Table 1b). Fractional solubility of modeled P in deposition ranges from 5% to
514 15%, with Saharan and Australian dust sources having solubilities averaging ~10%, consistent with Baker et al.
515 (2006a;2006b). Previous observations suggest a fractional solubility for P of 7-100% [e.g., Graham and Duce,
516 1982; Chen et al., 1985; Bergametti et al., 1992; Herut et al., 1999, 2002; Ridame and Guieu, 2002]. Fractional
517 solubility of Fe is 0.8%-1.2% in regions (Fig.14) where clay minerals such as illite play an important role
518 (Journet et al., 2008) with a mean value of 1.17% of fractional Fe solubility (Table 1b). There is an obvious
519 North-South gradient in the distribution of fractional solubility for Fe and Al, but with opposing magnitude
520 (Fig.14). The fractional solubility could not be calculated using Sol-2 (Sillanpaa method) since total elemental
521 fractions in soil were not reported in Sillanpaa (1982). Thus, the proportions of soluble Fe and K in total dust
522 using two methods are compared with each other. This shows similar distribution patterns but the values are
523 different (Fig. 15). The mineral method resulted in lower soluble Ca deposition and higher soluble Mg, P, Mn
524 (Fig. 15). Our results suggest significant differences in the spatial distribution of solubility depending on which
525 dataset is used to estimate soil solubility of elements. It should be noted that the solubility measurements by
526 Sillanpaa (1982) were performed at different pH values (pH of 7 vs. 2) and media of extraction (acidified
527 ultrapure waters vs. organic ligand solutions). It is known that pH and organic complexation greatly influence
528 the fractional solubility, at least for Fe (e.g. Paris et al., 2011). Thus, that would explain the differences in
529 elemental solubility that we computed for the dust. The soluble elemental deposition over ocean basins and ice
530 sheets are determined using two methods and are listed in Table 5. Annual inputs of soluble Mg, P, Ca, Mn, Fe
531 and K from mineral dust using method Sol-1 (Sol-2) were 0.28 (0.30) Tg, 16.89 (7.52) Gg, 1.32 (3.35) Tg,
532 22.84 (6.95) Gg, 0.068 (0.06) Tg, and 0.15 (0.25) Tg to oceans and ice sheets.

533 **Fig.13 Percentages of elements in dust deposition (%) after tuning. It is tuned based on original percentages of elements in**
534 **dust deposition in Fig. S1 by ratioing Obs./Mod. ratios listed in Table 3. Si did not change because there are not enough**
535 **observational data available**

536 **Fig. 14 Fractional solubility of elements (soluble element / total element) in dust deposition (%):a. Mg, b. P, c. Ca, d. Mn, e.**
537 **Fe, f. K, g. Al, h. Si**

538 **Fig. 15 Percentages of soluble elements in total dust deposition using(a) Sol-1 & (b) Sol-2 (%), Sol-1 refer to mineral method**
539 **after tuning, Sol-2 refer to Sillanpaa method described in the methods section (2).**

540 **Table 4 Deposition of dust elements into different ocean basins and glaciers**

541 **4 Summary and Conclusions**

542 A new technique combining soil and mineralogical datasets is introduced to estimate the global emission
543 inventory of soil associated elements Mg, P, Ca, Mn, Fe, K, Al, and Si. The spatial elemental dust emissions,
544 transport and deposition are simulated using CESM from 2001-2010. Spatial variability of soil element
545 fractions is characterized globally (Fig 2), and shows that the use of a constant element fraction in dust across
546 the globe is not consistent with existing observational data for Ca and Al (Fig 10 and 11). There are few
547 observations for elemental distributions in source regions to verify these emission, concentration and
548 deposition simulations, but for some elements (Ca and Al), the soil elemental distribution combined with the
549 transported dust flux in the model better captures the percentage of chemical elements in dust concentrations
550 observed (Figure 10, 11). However, both Mg and Mn levels are underestimated by the model using the present
551 mineral maps. The correlation of the percentage of elements at different sites is not statistically significant for
552 several elements (Mg, Mn, P and K), suggesting that improvements in the soil inventories or simulations is
553 required, although these results could also be due to low numbers of observations. The observations and model
554 results suggest the elemental fractions in dust varied globally and between different dust production regions,
555 especially for Ca with values from 1% to 30%. The ratio of Ca/Al, ranged between 0.1-5.0, and is confirmed as
556 an indicator of dust source regions (Zhang et al., 1997; Zhang et al., 2003; Sun et al., 2004a,b; Shen et al.,
557 2007). For Fe in TSP, the median of modeled fraction is 2.90%, less than the commonly assumed 3.5% Fe
558 used in dust models (e.g. Luo et al., 2008; Mahowald et al., 2008).

559 Seasonal variability of emission, concentration and deposition of most elements are simulated in the model.
560 Also, different soluble elemental datasets show that the fractional solubility of elements varies spatially.
561 Mineral dust element deposition fluxes into ocean basins are updated using a variable fractional elemental
562 inventory and could have potentially important impacts on evaluating their biogeochemical effects. This study
563 shows that soil emission inventories do a fairly good job at predicting dust elemental concentrations during
564 dust events, except for Mg and Mn. However, the high spatial heterogeneity in elemental distributions is not
565 captured in the model. Several sources of uncertainties exist in the model projections, the largest of which is
566 likely to be the assumptions in the soil mappings from soil types to minerals to elemental distributions. In the
567 future, these dust emission inventories can be combined with anthropogenic elemental inventories to further
568 improve our understanding of elemental deposition to the oceans.

569 **Acknowledgements**

570 We would like to thank the US Department of Defense (DOD) for sharing chemical data from their Enhanced
571 Particulate Matter Surveillance Program (EPMS), and anonymous reviewers for helpful comments. We
572 acknowledge the support of NSF grant 0932946 and 1137716 and DOE-SC0006735. Simulations were
573 conducted on the NSF National Center for Atmospheric Research's supercomputers.

574

575 Reference

- 576 Albani, S., Mahowald, N. M., Perry, A. T., Scanza, R. A., Zender, C. S., Heavens, N. G., Maggi, V., Kok, J. F.,
577 and Otto-Bliesner, B. L.: Improved dust representation in the Community Atmosphere Model, *J. Adv. Model. Earth*
578 *Syst.*, 6, 541–570, doi:10.1002/2013MS000279, 2014.
- 579 Astitha, M., Lelieveld, J., Abdel Kader, M., Pozzer, A., and de Meij, A.: Parameterization of dust emissions in the
580 global atmospheric chemistry-climate model EMAC: impact of nudging and soil properties, *Atmos. Chem. Phys.*, 12,
581 11057–11083, doi:10.5194/acp-12-11057-2012, 2012.
- 582 Baker, A. R., Kelly, S. D., Biswas, K. F., Witt, M., and Jickells, T. D.: Atmospheric deposition of nutrients to the
583 Atlantic Ocean, *Geophys. Res. Lett.*, 30, 2296, doi:10.1029/2003GL018518, 2003.
- 584 Baker, A. R., French, M., and Linge, K. L.: Trends in aerosol nutrient solubility along a west–east transect of the
585 Saharan dust plume, *Geophys. Res. Lett.*, 33, L07805, doi:10.1029/2005GL024764, 2006a.
- 586 Baker, A. R., Jickells, T. D., Witt, M., and Linge, K. L.: Trends in the solubility of iron, aluminum, manganese and
587 phosphorus collected over the Atlantic Ocean, *Mar. Chem.*, 98, 43–58, doi:10.1016/j.marchem.2005.06.004, 2006b.
- 588 Baker, A. R. and Croot, P. L.: Atmospheric and marine controls on aerosol iron solubility in seawater, *Mar. Chem.*,
589 120, 4–13, 2010.
- 590 Bergametti, G., Gomes, L., Coudé-Gaussen, G., Rognon, P. and Le Coustumer, M.: African dust observed over
591 Canary Islands: Source-regions identification and transport pattern for some summer situations, *J. Geophys. Res.*,
592 12, 14855–14864, doi:10.1029/JD094iD12p14855.1989.
- 593 Bergametti, G., Remoudaki, E., Losno, R., Steiner, E., Chatenet, B., and Buat-Menard, P.: Source, transport and
594 deposition of atmospheric phosphorus over the northwestern Mediterranean, *J. Atmos. Chem.*, 14, 501–513,
595 doi:10.1007/BF00115254, 1992.
- 596 Boyd, P., Wong, C., Merrill, J., Whitney, F., Snow, J., Harrison, P., and Gower, J.: Atmospheric iron supply and
597 enhanced vertical carbon flux in the NE subsarctic Pacific: is there a connection? *Global Biogeochem. Cy.*, 12, 429–
598 441, 1998.
- 599 Buck, C., Landing, W. M., Resing, J. A., and Lebon, G.: Aerosol iron and aluminum solubility in the northwest
600 Pacific Ocean: results from the 2002 IOC Cruise, *Geochem. Geophys. Geosy.*, 7, Q04M07,
601 doi:10.1029/2005GC000977, 2006.
- 602 Capone, D. G., Zehr, J. P., Paerl, H. W., Bergman, B., and Carpenter, E. J.: Trichodesmium, a globally significant
603 marine cyanobacterium, *Science*, 276, 1221–1229, 1997.
- 604 Carpenter, L. J., Fleming, Z. L., Read, K. A., Lee, J. D., Moller, S. J., Hopkins, J. R., Purvis, R. M., Lewis, A. C.,
605 Müller, K., Heinold, B., Herrmann, H., Fomba, K. W., Pinxteren, D. v., Müller, C., Tegen, I., Wiedensohler, A.,
606 Müller, T., N. Niedermeier, Achterberg, E. P., Patey, M. D., Kozlova, E. A., Heimann, M., Heard, D. E., Plane, J. M.
607 C., Mahajan, A., Oetjen, H., Ingham, T., Stone, D., Whalley, L. K., Evans, M. J., Pilling, M. J., Leigh, R. J., Monks,
608 P. S., Karunaharan, A., Vaughan, S., Arnold, S. R., Tschirner, J., Pöhler, D., Frieß, U., Holla, R., Mendes, L. M.,
609 Lopez, H., Faria, B., Manning, A. J., and Wallace, D. W. R.: Seasonal characteristics of tropical marine boundary
610 layer air measured at the Cape Verde Atmospheric Observatory, *J. Atmos. Chem.*, 67, 87–140, doi:10.1007/s10874-
611 011-9206-1, 2010.
- 612 Castillo, S., Moreno, T., Querol, X., Alastuey, A., Cuevas, E., Herrmann, L., Monkaila, M., and Gibbons, W.: Trace
613 element variation in size-fractionated African desert dusts, *J. Arid Environ.* 72, 1034–1045, 2008.
- 614 Chen, L., Arimoto R., and Duce R. A.: The sources and forms of phosphorus in marine aerosol particles and rain
615 from Northern New Zealand, *Atmos. Environ.*, 19, 779–787, 1985.

616 Chen, H.-Y., Fang, T.-H., Preston, M., and Lin, S.: Characterization of phosphorus in the aerosol of a coastal
617 atmosphere: using an sequential extraction method, *Atmos. Environ.*, 40, 279–289,
618 doi:10.1016/j.atmosenv.2005.09.051, 2006.

619 Chen, Y. and Siefert, R.: Seasonal and spatial distributions and dry deposition fluxes of atmospheric total and labile
620 iron over the tropical and subtropical North Atlantic Ocean, *J. Geophys. Res.*, 109, D09305,
621 doi:10.1029/2003JD003958, 2004.

622 Chen, Y., Paytan, A., Chase, Z., Measures, C., Beck, A. J., Sañudo-Wilhelmy, S. A., and Post, A. F.: Sources and
623 fluxes of atmospheric trace elements to the Gulf of Aqaba, Red Sea, *J. Geophys. Res.*, 113, D05306,
624 doi:10.1029/2007JD009110, 2008.

625 Claquin, T., Schulz, M., and Balkanski, Y. J.: Modeling the mineralogy of atmospheric dust sources, *J. Geophys.*
626 *Res.*, 104, 22243–22256, 1999.

627 Cohen, D. D., Stelcer, E., Hawas, O., and Garton, D.: IBA methods for characterisation of fine particulate
628 atmospheric pollution: a local, regional and global research problem, *Nucl. Instrum. Meth. B*, 219, 145–152, 2004.

629 Cohen, D. D., Stelcer, E., Garton, D., and Crawford, J.: Fine particle characterization, source apportionment and
630 long range dust transport into the Sydney Basin: a long term study between
631 1998 and 2009, *Atmospheric Pollution Research*, 2, 182–189, 2011.

632 Desboeufs, K., Journet, E., Rajot, J.-L., Chevaillier, S., Triquet, S., Formenti, P., and Zakou, A.: Chemistry of rain
633 events in West Africa: evidence of dust and biogenic influence in convective systems, *Atmos. Chem. Phys.*, 10,
634 9283–9293, doi:10.5194/acp-10-9283-2010, 2010.

635 Duce, R. A. and Tindale, N. W.: Atmospheric transport of iron and its deposition in the ocean, *Limnol. Oceanogr.*,
636 36, 1715–1726, 1991.

637 Christian, J.R. Advection in plankton models with variable elemental ratios. *Ocean Dynamics*, 57(1), 63-71.
638 doi:10.1007/s10236-006-0097-7, 2007.

639 Duce, R. A., Liss, P. S., Merrill, J. T., Atlas, E. L., Buat-Meard, P., Hicks, B. B., Miller, J. M., Prospero, J. M.,
640 Arimoto, R., Church, T. M., Ellis, W., Galloway, J. N., Hansen, L., Jickels, T. D., Knap, A. H., Reinhardt, K. H.,
641 Schneider, B., Soudine, A., Tokos, J. J., Tsunogai, S., Wollast, R., and Zhou, M.: The atmospheric input of trace
642 species to the world ocean, *Global Biogeochem. Cy.*, 5, 193–259, 1991.

643 Engelbrecht, J., McDonald, E., Gillies, J., Jayanty, R. K. M., Casuccio, G., and Gertler, A. W.: Characterizing
644 mineral dusts and other aerosols from the Middle East – Part 1: Ambient sampling, *Inhal. Toxicol.*, 21, 297–326,
645 2009.

646 Engelbrecht, J. P., Menendez, I., and Derbyshire, E.: Sources of PM_{2.5} impacting on Gran Canaria, Spain, *Catena*,
647 117, 119–132, doi:10.1016/j.catena.2013.06.017, 2014.

648 FAO-Unesco: Soil Map of the World, Southeast Asia, 1976, Sheet IX, Edition I, 1976.

649 Formenti, P., Rajot, J. L., Desboeufs, K., Caquineau, S., Chevaillier, S., Nava, S., Gaudichet, A., Journet, E., Triquet,
650 S., Alfaro, S., Chiari, M., Haywood, J., Coe, H., and Highwood, E.: Regional variability of the composition of
651 mineral dust from western Africa: results from the AMMA SOP0/DABEX and DODO field campaigns, *J. Geophys.*
652 *Res.*, 113, D00C13,
653 doi:10.1029/2008JD009903, 2008.

654 Formenti, P., Schütz, L., Balkanski, Y., Desboeufs, K., Ebert, M., Kandler, K., Petzold, A., Scheuven, D.,
655 Weinbruch, S., and Zhang, D.: Recent progress in understanding physical and chemical properties of African and
656 Asian mineral dust, *Atmos. Chem. Phys.*, 11, 8231–8256, doi:10.5194/acp-11-8231-2011, 2011.

657 Fung, I., Meyn, S. K., Tegen, I., Doney, S., John, J., and Bishop, J.: Iron supply and demand in the upper ocean,
658 *Global Biogeochem. Cy.*, 14, 281–295, 2000.

659 Gaudichet, A., Echalar, F., Chatenet, B., Quisefit, J. P., Malingre, G., Cachier, H., Buatmenard, P., Artaxo, P., and
660 Maenhaut, W.: Trace elements in tropical African savanna biomass burning aerosols, *J. Atmos. Chem.*, 22, 19–39,
661 1995.

662 Gold, C. M., Cavell, P. A., and Smith, D. G. W.: Clay minerals in mixtures: sample preparation, analysis, and
663 statistical interpretation, *Clay. Clay Miner.*, 3, 191–199, 1983.

664 Goudie, A. S. and Middleton, N. J.: *Desert Dust in the Global System*, Springer, Berlin, 2006.

665 Graham, W. F. and Duce, R. A.: The atmospheric transport of phosphorus to the western North Atlantic, *Atmos.*
666 *Environ.*, 16, 1089–1097, doi:10.1016/0004-6981(82)90198-6, 1982.

667 Guieu, C., Bonnet, S., Wagener, T., and Loye-Pilot, M.-D.: Biomass burning as a source of dissolved iron to the
668 open ocean?, *Geophys. Res. Lett.*, 22, L19608, doi:10.1029/2005GL022962, 2005.

669 Guo, L., Chen, Y., Wang, F. J., Meng, X., Xu, Z. F., and Zhuang, G.: Effects of Asian dust on the atmospheric input
670 of trace elements to the East China Sea, *Mar. Chem.*, 163, 19–27, doi:10.1016/j.marchem.2014.04.003, 2014.

671 Hand, J. L., Mahowald, N. M., Chen, Y., Siefert, R. L., Luo, C., Subramaniam, A., and Fung, I.: Estimates of
672 atmospheric-processed soluble iron from observations and a global mineral aerosol model: Biogeochemical
673 implications, *J. Geophys. Res.*, 109, D17205, doi:10.1029/2004JD004574, 2004.

674 Herut, B., Krom, M., Pan, G., and Mortimer, R.: Atmospheric input of nitrogen and phosphorus to the southeast
675 Mediterranean: sources, fluxes and possible impact, *Limnol. Oceanogr.*, 44, 1683–1692, 1999.

676 Herut, B., Collier, R., and Krom, M.: The role of dust in supplying nitrogen and phosphorus to the southeast
677 Mediterranean, *Limnol. Oceanogr.*, 47, 870–878, 2002.

678 Herut, B., Zohary, T., Krom, M. D., Mantoura, R. F. C., Pitta, V., Psarra, S., Rassoulzadegan, F., Tanaka, T., and
679 Thingstad, F. T.: Response of east Mediterranean surface water to Saharan dust: on-board microcosm experiment
680 and field observations, *Deep-Sea Res. Pt. II*, 52, 3024–3040, doi:10.1016/j.dsr2.2005.09.003, 2005.

681 Hinkley, T. K., Lamothe, P. J., Wilson, S. A., Finnegan, D. L., and Gerlach, T. M.: Metal emissions from Kilauea,
682 and a suggested revision of the estimated worldwide metal output by quiescent degassing of volcanoes, *Earth Planet.*
683 *Sc. Lett.*, 170, 315–325, 1999.

684 Huneus, N., Schulz, M., Balkanski, Y., Griesfeller, J., Prospero, J., Kinne, S., Bauer, S., Boucher, O., Chin, M.,
685 Dentener, F., Diehl, T., Easter, R., Fillmore, D., Ghan, S., Ginoux, P., Grini, A., Horowitz, L., Koch, D., Krol, M. C.,
686 Landing, W., Liu, X., Mahowald, N., Miller, R., Morcrette, J.-J., Myhre, G., Penner, J., Perlwitz, J., Stier, P.,
687 Takemura, T., and Zender, C. S.: Global dust model intercomparison in AeroCom phase I, *Atmos. Chem. Phys.*, 11,
688 7781–7816, doi:10.5194/acp-11-7781-2011, 2011.

689 Jeong, G. Y.: Bulk and single-particle mineralogy of Asian dust and a comparison with its source soils, *J. Geophys.*
690 *Res.*, 113, D02208, doi:10.1029/2007jd008606, 2008.

691 Jickells, T., An, Z., Andersen, K., Baker, A., Bergametti, G., Brooks, N., Cao, J., Boyd, P., Duce, R., Hunter, K.,
692 Kawahata, H., Kubilay, N., LaRoche, J., Liss, P., Mahowald, N., Prospero, J., Ridgwell, A., Tegen, I., and Torres, R.:
693 Global iron connections between dust, ocean biogeochemistry and climate, *Science*, 308, 67–71, 2005.

694 Journet, E., Desboeufs, K. V., Caquineau, S., and Colin, J.-L.: Mineralogy as a critical factor of dust iron solubility,
695 *Geophys. Res. Lett.*, 35, L07805, doi:10.1029/2007gl031589, 2008.

696 Journet, E., Balkanski, Y., and Harrison, S. P.: A new data set of soil mineralogy for dust-cycle modeling, *Atmos.*
697 *Chem. Phys.*, 14, 3801–3816, doi:10.5194/acp-14-3801-2014, 2014.

698 Kandler, K., Benker, N., Bundke, U., Cuevas, E., Ebert, M., Knippertz, P., Rodríguez, S., Schütz, L., and Weinbruch,
699 S.: Chemical composition and complex refractive index of Saharan mineral dust at Izaña, Tenerife (Spain) derived
700 by electron microscopy, *Atmos. Environ.*, 41, 8058–8074, 2007.

701 Kok, J. F.: A scaling theory for the size distribution of emitted dust aerosols suggests climate models underestimate
702 the size of the global dust cycle, *P. Natl. Acad. Sci. USA*, 108, 1016–021, 2011.

703 Kreutz, K. J. and Sholkovitz, E. R.: Major element, rare earth element, and sulfur isotopic composition of a high-
704 elevation firn core: sources and transport of mineral dust in central Asia, *Geochem. Geophys. Geos.*, 1, 1048–1071,
705 2000.

706 Lam, P. and Bishop, J.: The continental margin is a key source of iron to the North Pacific Ocean, *Geophys. Res.
707 Lett.*, 35, L07608, doi:10.1029/2008GL033294, 2008.

708 Lawrence, C. R. and Ne, J. C.: The physical and chemical flux of eolian dust across the landscape: a synthesis of
709 observations and an evaluation of spatial patterns, *Chem. Geol.*, 267, 46–63, doi:10.1016/j.chemgeo.2009.02.005,
710 2009.

711 Li, G., Chen, J., Chen, Y., Yang, J., Ji, J., and Liu, L.: Dolomite as a tracer for the source regions of Asian dust, *J.
712 Geophys. Res.*, 112, D17201, doi:10.1029/2007jd008676, 2007.

713 Lin, S.-J., and R. B. Rood. An explicit flux-form semi-Lagrangian shallow-water model on the sphere, *Quarterly
714 Journal of the Royal Meteorological Society*, 123, 2477-2498, 1997.

715 Luo, C., Mahowald, N., Bond, T., Chuang, P. Y., Artaxo, P., Siefert, R., Chen, Y., and Schauer, J.: Combustion
716 iron distribution and deposition, *Global Biogeochem. Cy.*, 22, GB1012, doi:10.1029/2007GB002964, 2008.

717 Mahowald, N.; Baker, A.; Bergametti, G.; Brooks, N.; Duce, R.; Jickells, T.; Kubilay, N.; Prospero, J.; Tegen, I.
718 Atmospheric global dust cycle and iron inputs to the ocean, *Global Biogeochem. Cy.*, 19, GB4025,
719 doi:10.1029/2004GB002402, 2005.

720 Mahowald, N., Muhs, D. R., Levis, S., Rasch, P. J., Yoshioka, M., Zender, C. S., and Luo, C.: Change in
721 atmospheric mineral aerosols in response to climate: last glacial period, preindustrial, modern, and doubled carbon
722 dioxide climates, *J. Geophys. Res.-Atmos.*, 111, D10202, doi:10.1029/2005JD006653, 2006.

723 Mahowald, N., Jickells, T. D., Baker, A. R., Artaxo, P., Benitez-Nelson, C. R., Bergametti, G., Bond, T. C., Chen,
724 Y., Cohen, D. D., Herut, B., Kubilay, N., Losno, R., Luo, C., Maenhaut, W., McGee, K. A., Okin, G. S., Siefert, R.
725 L., and Tsukuda, S.: Global distribution of atmospheric phosphorus sources, concentrations and deposition rates, and
726 anthropogenic impacts, *Global Biogeochem. Cy.*, 22, GB4026, doi:10.1029/2008GB003240, 2008.

727 Marino, F., Maggi, V., Delmonte, B., Ghermandi, G., and Petit, J. R.: Elemental composition (Si, Fe, Ti) of
728 atmospheric dust over the last 220 kyr from the EPICA ice core (Dome C, Antarctica), *Ann. Glaciol.*, 39, 110–118,
729 doi:10.3189/172756404781813862, 2004.

730 Marteel, A., Gaspari, V., Boutron, C. F., Barbante, C., Gabrielli, P., Cescon, P., Ferrari, C., Dommergue, A.,
731 Rosman, K., Hong, S., and Hur, S.: Climate-related variations in crustal trace elements in Dome C (East Antarctica)
732 ice during the past 672 kyr, *Climatic Change*, 92, 191–211, 2009.

733 Martin, J. H., Gordon, R. M., and Fitzwater, S. E.: The case for iron, *Limnol. Oceanogr.*, 36, 1793–1802, 1991.

734 Measures, C. and Vink, S.: On the use of dissolved aluminum in surface waters to estimate dust deposition to the
735 ocean, *Global Biogeochem. Cy.*, 14, 317–327, 2000.

736 Mermut, A. R. and Cano, A. F.: Baseline studies of the clay minerals society source clays: chemical analyses of
737 major elements, *Clay. Clay Miner.*, 49, 381–386, 2001.

738 Mills, M. M., Ridame, C., Davey, M., LaRoche, J., and Geider, R.: Iron and phosphorus co-limit nitrogen fixation in

739 the eastern tropical North Atlantic, *Nature*, 429, 292–294, 2004.

740 Moore, J. K. and Braucher, O.: Sedimentary and mineral dust sources of dissolved iron to the world ocean,
741 *Biogeosciences*, 5, 631–656, doi:10.5194/bg-5-631-2008, 2008.

742 Morel, F. M. M., Milligan, A. J., and Saito, M. A.: Marine bioinorganic chemistry: the role of trace metals in the
743 oceanic cycles of major nutrients, in: *Treatise on Geochemistry*, Vol. 6., Elsevier, Pergamon, Oxford, 113–143,
744 ISBN 0-08-043751-6, 2003.

745 Moreno, T., Querol, X., Castillo, S., Alastuey, A., Cuevas, E., Herrmann, L., Mounkaila, M., Elvira, J., and Gibbons,
746 W.: Geochemical variations in aeolian mineral particles from the Sahara-Sahel dust corridor, *Chemosphere*, 65,
747 261–270, 2006.

748 Nickovic, S., Vukovic, A., Vujadinovic, M., Djurdjevic, V., and Pejanovic, G.: Technical Note: High-resolution
749 mineralogical database of dust-productive soils for atmospheric dust modeling, *Atmos. Chem. Phys.*, 12, 845–855,
750 doi:10.5194/acp-12-845-2012, 2012.

751 Nickovic S., Vukovic A., Vujadinovic M. (2013). Atmospheric processing of iron carried by mineral dust.
752 *Atmos. Chem. Phys.*, 13,9169–9181, doi:10.5194/acp-13-9169-2013, 2013.

753 Nozaki, Y.: A fresh look at element distribution in the North Pacific, *EOS T. Am. Geophys. Un.*,78, 221–221,
754 doi:10.1029/97EO00148, 1997.

755 Okin, G. S., Mahowald, N., Chadwick, O. A., and Artaxo, P.: Impact of desert dust on the biogeochemistry
756 Of phosphorus in terrestrial eco-systems, *Global Biogeochem. Cy.*, 18, GB2005, doi:10.1029/2003GB002145, 2004.

757 Paris, R., Desboeufs, K. V., Formenti, P., Nava, S., and Chou, C.: Chemical characterization of iron in dust and
758 biomass burning aerosols during AMMA-SOP0/DABEX: implication for iron solubility, *Atmos. Chem. Phys.*, 10,
759 4273–4282, doi:10.5194/acp-10-4273-2010, 2010.

760 Paytan, A., Mackey, K., Chen, Y., Lima, I., Doney, S., Mahowald, N., Lablosa, R., and Post, A.: Toxicity of
761 atmospheric aerosols on marine phytoplankton, *P. Natl. Acad. Sci. USA*, 106, 106, 4601–4605,
762 doi:10.1073/pnas.0811486106, 2009.

763 Perry, K. D., Cahill, T. A., Eldred, R. A., Dutcher, D. D., and Gill, T. E.: Long-range transport of North African dust
764 to the eastern United States, *J. Geophys. Res.-Atmos.*, 102, 11225–11238, 1997.

765 Petrucci, R. H., Harwood, W. S., Herring, G., Madura, J.: *General Chemistry: Principles and Modern Application*,
766 9th edn., Printice Hall, New Jersey, Pearson2001.

767 Prospero, J. M., Landing, W. M., and Schulz, M.: African dust deposition to Florida: temporal and spatial variability
768 and comparisons to models, *J. Geophys. Res.*, 115, D13304,doi:10.1029/2009JD012773, 2010.

769 Rasch, P., D. Coleman, N. Mahowald, D. Williamson, S.-J. Lin, B. Boville, and P. Hess. Characteristics of
770 atmospheric transport using three numerical formulations for atmospheric dynamics in a single GCM framework,
771 *Journal of Climate*, 19, 2243-2266, 2006.

772

773 Reheis, M. C. and Kihl, R.: Dust deposition in southern Nevada and California, 1984–1989 –relations to climate,
774 source area, and source lithology, *J. Geophys. Res.-Atmos.*, 100, 8893–8918, 1995.

775 Reid, E. A., Reid, J. S., Meier, M. M., Dunlap, M. R., Cli_ , S. S., Broumas, A., Perry, K., and Maring, H.:
776 Characterization of African dust transported to Puerto Rico by individual particle and size segregated bulk analysis,
777 *J. Geophys. Res.*, 108, 8591, doi:10.1029/2002JD002935, 2003.

778 Ridame, C. and Guieu, C.: Saharan input of phosphate to the oligotrophic water of the open western Mediterranean

779 Sea, *Limnol. Oceanogr.*, 47, 856–869, 2002.

780 Scanza, R. A., Mahowald, N., Ghan, S., Zender, C. S., Kok, J. F., Liu, X., and Zhang, Y.: Modeling dust as
781 component minerals in the Community Atmosphere Model: development of framework and impact on radiative
782 forcing, *Atmos. Chem. Phys.* 15, 537-561, 2015.

783 Schütz, L. and Rahn, K. A.: Trace element concentrations in erodible soils, *Atmos. Environ.*, 16, 171–176, 1982.

784 Seinfeld, J. H. and Pandis, S. N.: *Atmospheric Chemistry and Physics: from Air Pollution to Climate Change*, J.
785 Wiley, New York, 1998.

786 Shao, Y.: A model for mineral dust emission, *J. Geophys. Res.*, 106, 20239–20254, doi:10.1029/2001jd900171,
787 2001.

788 Shen, Z. X., Li, X., Cao, J., Caquineau, S., Wang, Y., and Zhang, X.: Characteristics of clay minerals in Asian dust
789 and their environmental significance, *China Part.*, 3, 260–264, 2005.

790 Shen, Z. X., Cao, J., Li, X., Okuda, T., Wang, Y., and Zhang, X.: Mass concentration and mineralogical
791 characteristics of aerosol particles collected at Dunhuang during ACE-Asia, *Adv. Atmos. Sci.*, 23, 291–298, 2006.

792 Shen, Z. X., Cao, J. J., Arimoto, R., Zhang, R. J., Jie, D. M., Liu, S. X., Zhu, C.S.: Chemical composition and
793 source characterization of spring aerosol over Horqin sand land in northeastern China, *J. Geophys. Res.*, 112,
794 D14315, doi:10.1029/2006JD007991, 2007.

795 Sillanpää, M.: *Micronutrients and the Nutrient Status of Soils: a Global Study*, FAO Soils Bulletin, No. 48.,
796 Appendix 6–7, Rome, 1982.

797 Stoorvogel, J. J., VanBreemen, N., and Janssen, B. H.: The nutrient input by Harmattan dust to a forest ecosystem in
798 Côte d’Ivoire, Africa, *Biogeochemistry*, 37, 145–157, 1997.

799 Sun, Y., Zhuang, G., Yuan, H., Zhang, X., and Guo, J.: Characteristics and sources of 2002 super dust storm in
800 Beijing, *Chinese Sci. Bull.*, 49, 698–705, 2004a.

801 Sun, Y., Zhuang, G., Wang, Y., Han, L., Guo, J., Dan, M., Zhang, W., Wang, Z., and Hao, Z.: The air-borne
802 particulate pollution in Beijing – concentration, composition, distribution and sources, *Atmos. Environ.*, 38, 5991–
803 6004, 2004b.

804 Svensson, A., Biscaye, P. E., and Grousset, F. E.: Characterization of late glacial continental dust in the Greenland
805 Ice Core Project ice core, *J. Geophys. Res.*, 105, 4637–4656, doi:10.1029/1999jd901093, 2000.

806 Swap, R., Garstang, M., Greco, S., Talbot, R., and Kallberg, P.: Saharan dust in the Amazon Basin, *Tellus B*, 44,
807 133–149, 1992.

808 Textor, C., Schulz, M., Guibert, S., Kinne, S., Balkanski, Y., Bauer, S., Berntsen, T., Berglen, T., Boucher, O., Chin,
809 M., Dentener, F., Diehl, T., Easter, R., Feichter, H., Fillmore, D., Ghan, S., Ginoux, P., Gong, S., Grini, A.,
810 Hendricks, J., Horowitz, L., Huang, P., Isaksen, I., Iversen, I., Kloster, S., Koch, D., Kirkevåg, A., Kristjansson, J. E.,
811 Krol, M., Lauer, A., Lamarque, J. F., Liu, X., Montanaro, V., Myhre, G., Penner, J., Pitari, G., Reddy, S., Seland, Ø.,
812 Stier, P., Takemura, T., and Tie, X.: Analysis and quantification of the diversities of aerosol life cycles within
813 AeroCom, *Atmos. Chem. Phys.*, 6, 1777–1813, doi:10.5194/acp-6-1777-2006, 2006.

814 Textor, C., Schulz, M., Guibert, S., Kinne, S., Balkanski, Y., Bauer, S., Berntsen, T., Berglen, T., Boucher, O., Chin,
815 M., Dentener, F., Diehl, T., Feichter, J., Fillmore, D., Ginoux, P., Gong, S., Grini, A., Hendricks, J., Horowitz, L.,
816 Huang, P., Isaksen, I. S. A., Iversen, T., Kloster, S., Koch, D., Kirkevåg, A., Kristjansson, J. E., Krol, M., Lauer, A.,
817 Lamarque, J. F., Liu, X., Montanaro, V., Myhre, G., Penner, J. E., Pitari, G., Reddy, M. S., Seland, Ø., Stier, P.,
818 Takemura, T., and Tie, X.: The effect of harmonized emissions on aerosol properties in global models – an
819 AeroCom experiment, *Atmos. Chem. Phys.*, 7, 4489–4501, doi:10.5194/acp-7-4489-2007, 2007.

820 Titschack, J., Goetz-Neunhoefer, F., and Neubauer, J.: Magnesium quantification in calcites [(Ca,Mg)CO₃] by
821 Rietveld-based XRD analysis: revisiting a well-established method, *Am. Mineral.*, 96, 1028–1038, 2011.

822 Wang, Q., Zhuang, G., Li, J., Huang, K., Zhang, R., Jiang, Y., Lin, Y., and Fu, J. S.: Mixing of dust with pollution
823 on the transport path of Asian dust – revealed from the aerosol over Yulin, the north edge of Loess Plateau, *Sci.*
824 *Total Environ.*, 409, 573–581, 2010.

825 Werner, M., Tegen, I., Harrison, S. P., Kohfeld, K. E., Prentice, I. C., Balkanski, Y., Rodhe, H., and Roelandt, C.:
826 Seasonal and interannual variability of the mineral dust cycle under present and glacial climate conditions, *J.*
827 *Geophys. Res.*, 107, D244744, doi:10.1029/2002JD002365, 2002.

828 Wilke, B. M., Duke, B. J., and Jimoh, W. L. O.: Mineralogy and chemistry of Harmattan dust in northern Nigeria,
829 *Catena*, 11, 91–96, 1984.

830 Xuan, J., Sokolik, I. N., Hao, J., Guo, F., Mao, H., and Yang, G.: Identification and characterization of sources of
831 atmospheric mineral dust in East Asia, *Atmos. Environ.*, 38, 6239–6252, 2004.

832 Yadav, S. and Rajamani, V.: Geochemistry of aerosols of northwestern part of India adjoining the Thar Desert,
833 *Geochim. Cosmochim. Ac.*, 68, 1975–1988, 2004.

834 Zender, C., Bian, H., and Newman, D.: Mineral Dust Entrainment and Deposition (DEAD) model: description and
835 1990s dust climatology, *J. Geophys. Res.*, 108, 4416, doi:10.1029/2002JD002775, 2003.

836 Zhang, X. Y., Arimoto, R., and An, Z. S.: Dust emission from Chinese desert sources linked to variation in
837 atmospheric circulation, *J. Geophys. Res.*, 102, 28041–28047, 1997.

838 Zhang, X. Y., Arimoto, R., Zhu, G. H., Chen, T., and Zhang, G. Y.: Concentration, size distribution and deposition
839 of mineral aerosol over Chinese desert regions, *Tellus B*, 50, 317–330, 1998.

840 Zhang, X. Y., Gong, S. L., Shen, Z. X., Mei, F. M., Xi, X. X., Liu, L. C., Zhou, Z. J., Wang, D., Wang, Y. Q., and
841 Cheng, Y.: Characterization of soil dust aerosol in China and its transport and distribution during 2001 ACE-Asia: 1.
842 Network observations, *J. Geophys. Res.*, 108, 4261, doi:10.1029/2002jd002632, 2003.

843

844

Main Tables 1- 5

845

846 **Table1a Generalized mineral compositions (%) applied in this study**

847 **Table1b Elemental solubility as a percentage of the element contained in the minerals (%)**

848 **Table 2 Ten year averaged emission rates (Tg/yr) and percentages of elements over desert regions (%)**

849 **Table 3 Comparison of modeled and observed fractions of chemical elements in TSP and tuning ratio based**
850 **on 14-site measurements**

851 **Table 4 Percentage (%) of elements in dust deposition into different ocean basins and ice sheets***

852 **Table 5 Deposition of dust elements into different oceans and ice sheets***

853

854

855

856

857

858

Table1a Generalized mineral compositions (%) applied in this study

Mineral	Mg	P	Ca	Mn	Fe	Al	Si	K
Smectite	1.21	0.17	0.91	0.03	2.55	8.57	27.44	0.27
Illite	0.85	0.09	1.45	0.03	4.01	10.47	24.11	4.28
Hematite	0.09	0.18	0.12	0.07	57.50	2.67	2.11	0.07
Feldspar	0.15	0.09	3.84	0.01	0.34	10.96	25.24	5.08
Kaolinite	0.02	0.16	0.03	0.01	0.24	20.42	20.27	0.00
Calcite	0.00	0.00	40.00	0.00	0.00	0.00	0.00	0.00
Quartz	0.00	0.00	0.00	0.00	0.00	0.00	46.70	0.00
Gypsum	0.00	0.00	23.30	0.00	0.00	0.00	0.00	0.00

859

860

Table1b Elemental solubility as a percentage of the element contained in the minerals (%)

Mineral	Mg	P	Ca	Mn	Fe	Al	Si	K
Smectite	14.09	2.93	79.20	25.35	2.60	0.00	0.05	31.41
Illite	7.80	30.58	50.96	24.93	1.17	0.15	0.05	2.87
Hematite	0.00	0.00	0.00	3.39	0.01	0.00	0.00	0.00
Feldspar	5.17	0.00	4.46	4.71	3.01	0.12	0.02	4.53
Kaolinite	22.32	0.00	21.97	0.00	4.26	0.38	0.37	0.00
Calcite	0.00	0.00	7.00	0.00	0.00	0.00	0.00	0.00
Quartz	0.00	0.00	0.00	0.00	0.00	0.00	0.0003	0.00
Gypsum	0.00	0.00	0.56	0.00	0.00	0.00	0.00	0.00

861

862 *Fe content came from Journet et al. (2008), the other elements were from personal communication with E. Journet.

863

864

865

866

867 **Table 2 Ten year averaged emission rates (Tg/yr) and percentages of elements over desert**868 **regions (%)**

869 (For this table, annual mean emission of each element is divided by the annual mean emission of

870 dust to obtain the %.)

Source Regions	Mg	P	Ca	Mn	Fe	K	Al	Si	Dust
WAsia	0.91	1.77E-01	12.73	3.53E-02	5.53	3.70	16.71	72.43	251.17
NCAAsia	0.50	9.27E-02	6.05	1.80E-02	2.26	1.90	8.36	37.99	128.59
CAsia	0.13	2.54E-02	1.57	4.98E-03	0.70	0.55	2.35	9.77	33.82
SCAsia	0.05	1.07E-02	0.54	1.93E-03	0.29	0.22	1.04	4.07	13.91
EAsia	0.21	4.38E-02	1.62	8.16E-03	1.28	0.85	4.22	18.27	58.90
Asian Region	1.79	3.50E-01	22.52	6.84E-02	10.06	7.23	32.67	142.54	486.4
ESah	1.23	2.74E-01	11.98	4.83E-02	6.62	5.41	26.45	102.59	346.16
WSah	2.62	5.31E-01	30.67	1.01E-01	14.25	11.04	50.35	208.70	712.00
SNAf	0.02	1.17E-02	0.17	1.47E-03	0.37	0.12	1.25	4.33	13.98
SAf	0.01	3.10E-03	0.18	5.90E-04	0.11	0.06	0.31	1.34	4.46
Africa	3.89	8.20E-01	42.99	1.51E-01	21.34	16.63	78.36	316.96	1076.6
NWNAm	0.00002	4.70E-06	0.0001	8.00E-07	0.0002	0.0001	0.0005	0.0019	0.030
SWNAm	0.02	3.01E-03	0.16	6.00E-04	0.10	0.07	0.29	1.27	4.20
North America	0.02	3.02E-03	0.16	6.00E-04	0.10	0.07	0.29	1.27	4.2
SAm	0.0005	1.20E-04	0.01	2.00E-05	0.003	0.002	0.01	0.04	0.15
Patag	0.03	6.79E-03	0.27	1.32E-03	0.20	0.13	0.62	2.82	9.08
South America	0.03	6.91E-03	0.27	1.34E-03	0.21	0.13	0.63	2.86	9.2
WAstr	0.0005	1.30E-04	0.003	2.00E-05	0.003	0.002	0.01	0.05	0.16
EAstr	0.02	5.13E-03	0.20	9.10E-04	0.16	0.10	0.48	1.78	6.11
Australia region	0.02	5.26E-03	0.20	9.30E-04	0.17	0.10	0.49	1.83	6.3
Global	5.75	1.18E+00	66.14	2.22E-01	31.87	24.15	112.44	465.46	1582.7
Global mean % element	0.36	0.07	4.18	0.01	2.01	1.53	7.10	29.41	/
Min. % element in 15 SR*	0.17	0.07	1.19	0.01	1.67	0.86	6.50	28.84	/
Max. % element in 15 SR*	0.39	0.08	5.07	0.02	2.68	1.63	8.96	31.38	/

871 *SR refer to source regions

872

873 **Table 3 Comparison of modeled and observed fractions of chemical elements in TSP, and tuning**
 874 **ratio based on 13-site measurements. (For this table comparing the elemental ratios at the**
 875 **measurement sites, the % value at each time measured is averaged across time and space for this**
 876 **comparison.)**

	Mg	P	Ca	Mn	Fe	K	Al
Corr. coeff. Of Averaged Fractions	0.14	-0.32	0.75	-0.51	0.29	-0.16	0.72
Median of Obs. (%)	1.45	0.09	5.42	0.070	3.10	1.79	5.26
Median of Mod.(%)	0.43	0.08	3.41	0.020	2.29	1.54	7.81
Obs./Mod. Median Ratio (tuned ratio)	3.4	1.1	1.6	3.5	1.4	1.2	0.7

877

878

879 **Table 4 Percentage (%) of elements in dust deposition into different ocean basins and ice sheets***

Ocean Basins/Glacier	Mg	P	Ca	Mn	Fe	K	Al	Si**
North Atlantic	1.43	0.10	5.36	0.06	3.05	1.89	5.96	28.32
South Atlantic	1.50	0.10	5.36	0.06	3.35	1.84	6.01	28.07
North Pacific	1.56	0.10	5.92	0.06	3.26	1.90	5.78	28.01
South Pacific	1.47	0.10	5.30	0.06	3.87	1.86	6.15	27.61
North Indian	1.38	0.08	7.90	0.05	3.13	1.81	4.95	28.29
South Indian	1.53	0.10	6.50	0.06	3.64	1.87	5.88	27.33
Southern Ocean	1.56	0.10	5.12	0.06	3.74	1.88	5.88	28.25
Arctic	1.60	0.10	6.23	0.06	3.31	1.96	5.76	27.76
Mediterranean	1.37	0.08	7.14	0.05	2.90	1.88	4.85	29.14
Antarctic ice sheets	1.50	0.10	4.90	0.06	3.54	1.82	5.55	29.17
Greenland ice sheets	1.50	0.09	7.49	0.06	2.82	1.89	5.24	28.00
Averaged	1.49	0.10	6.11	0.06	3.33	1.87	5.64	28.18

880 *After timing tuned ratios (Table 3) except for Si

881 ** Not tuning

882 (For this table, annual mean deposition of each element is divided by the annual mean deposition of
 883 dust to obtain the %.)

884

885

886

Table 5 Deposition of dust elements into different oceans and ice sheets *

Ocean / ice sheet	Mg (Tg/yr)		P (Gg/yr)		Ca (Tg/yr)		Mn (Gg/yr)		Fe (Tg/yr)		K (Tg/yr)							
	Sol-1	Sol-2	Sol-1	Sol-2	Sol-1	Sol-2	Sol-1	Sol-2	Sol-1	Sol-2	Sol-1	Sol-2						
North Atlantic	1.50	0.16	0.14	103.12	8.81	4.10	5.64	0.68	1.81	58.90	12.08	3.87	3.20	0.036	0.033	1.99	0.008	0.136
South Atlantic	0.13	0.01	0.02	8.84	0.79	0.38	0.47	0.06	0.17	5.17	1.07	0.34	0.30	0.003	0.003	0.16	0.007	0.014
North Pacific	0.28	0.03	0.03	17.47	1.66	0.65	1.06	0.13	0.33	10.58	2.25	0.58	0.58	0.007	0.006	0.34	0.014	0.025
South Pacific	0.01	0.001	0.001	0.86	0.07	0.04	0.04	0.006	0.01	0.50	0.10	0.03	0.03	0.0003	0.000	0.02	0.0007	0.001
North Indian	0.56	0.06	0.06	34.38	3.54	1.52	3.23	0.29	0.63	21.86	4.62	1.35	1.28	0.013	0.013	0.74	0.03	0.049
South Indian	0.05	0.005	0.005	3.03	0.30	0.20	0.20	0.02	0.05	1.85	0.39	0.16	0.11	0.001	0.001	0.06	0.002	0.004
Southern Ocean	0.002	0.0003	0.0003	0.15	0.01	0.01	0.01	0.001	0.003	0.09	0.02	0.01	0.01	0.0001	0.0001	0.00	0.0001	0.0002
Arctic	0.02	0.002	0.0020	1.34	0.13	0.05	0.09	0.01	0.02	0.83	0.18	0.04	0.05	0.0005	0.0004	0.03	0.001	0.002
Mediterranean	0.18	0.02	0.02	10.66	1.07	0.36	0.92	0.09	0.22	6.76	1.42	0.36	0.37	0.004	0.004	0.24	0.011	0.017
Antarctic ice sheets	0.001	0.0001	0.0001	0.08	0.007	0.003	0.00	0.001	0.002	0.05	0.01	0.003	0.00	0.00003	0.00003	0.00	0.0001	0.0001
Greenland ice sheets	0.09	0.01	0.01	5.39	0.49	0.21	0.44	0.04	0.10	3.30	0.71	0.19	0.17	0.002	0.002	0.11	0.005	0.007
Total	2.83	0.30	0.28	185.32	16.89	7.52	12.11	1.32	3.35	109.89	22.84	6.95	6.10	0.068	0.06	3.69	0.153	0.25

887 *Here the soluble element deposition using Sol-1 has been tuned by timing tuned ratios (Table 3); Sol-1 refer to mineral method after tuning, Sol-2 refer to Stillampa method
888 described in the methods section (2).

889 Main Figures 1- 15

890 **Fig.1. Observational sites** (S1-Hetian, China; S2-Tazhong, China; S3-Yu Lin, China; S4-Duolun,
891 China; S5-Shengsi, China; S6-Hanoi, Vietnam; S7-Marnila, Philippines; S8- Balad, Iraq; S9-Balad,
892 Iraq; S10-Taji, Iraq; S11-Eilat; S12-Cape Verde Atmospheric Observatory (CVAO); S13-
893 Muswellbrook, Australia; S14-Richmond, Australia; S15-Tamanrasset, Algeria; S16-Banizoumbou,
894 Niger; S17-Douz, Tunisia) **and dust-producing regions** (WAsia: West Asia; NC-As: North Central
895 Asia; CAsia: Central Asia; SC-As: South Central Asia; EAsia:East Asia; WN-Af:North West Africa;
896 EN-Af: North East Africa; S-NAf: Southern North Africa; SAf: Southern Africa; MWNAm: Middle
897 North West America; SWNAm: Southern North West America; SAm1: Northern South America;
898 SAm2: Southern South America; WAus: West Australia; EAus: East Australia)

899 Fig.2 Global elemental distributions (in mass percentage) in a1: Clay Mg, a2: Clay P, a3: Clay Ca, a4: Clay Mn, a5:
900 Clay Fe, a6: Clay K, a7:., Clay Al, a8: Clay Si; b1: Silt Mg, b2: Silt P, b3: Silt Ca, b4: Silt Mn, b5: Silt Fe, b6: Silt
901 K, b7: Silt Al, b8: Silt Si.

902 Fig.3 Global mean elemental percentages in (a) four-bin dust emission and (b) clay and silt fractions of soils (Bin1-4
903 refer to particle range listed in Table S2, clay refer to < 2 μ m, silt refer to > 2 μ m)

904 Fig.4 Percentages of elements in dust concentration (mass %) : a. Mg, b. P, c. Ca, d. Mn, e. Fe, f. K, g. Al, h. Si.
905 Elemental % shown here are calculated using the annual mean element concentration divided by the annual mean
906 dust concentration.

907 Fig.5 Ratio of mass fractions of elements in dust deposition to that in atmospheric dust : a. Mg, b. P, c. Ca, d. Mn, e.
908 Fe, f. K, g. Al, h. Si. Elemental ratios shown here are calculated using the annual mean element deposition divided
909 by the annual mean dust deposition.

910 Fig.6 Ten-year monthly variability in mean of elemental percentages in atmospheric dust (mass %) : a. Mg, b. P, c.
911 Ca, d. Mn, e. Fe, f. K, g. Al, h. Si. Elemental monthly mean % are calculated using the monthly mean emission of
912 each element divided by the monthly mean emission of dust.

913 Fig.7 Ten-year monthly variability in mean of elemental percentages in dust deposition (mass %):a. Mg, b. P, c. Ca,
914 d. Mn, e. Fe, f. K, g. Al, h. Si. Elemental monthly mean % are calculated using the monthly mean emission of each
915 element divided by the monthly mean emission of dust.

916

917 Fig.8 Ca/Al in Soil and ten year averaged Ca/Al ratio in dust emission, concentration and deposition. Top two (a,b)
918 refer to ratio in clay and silt desert soil, middle one (c) refer to ratio in dust emission, and bottom two (d,e) refer to

919 ratio in dust concentration and deposition. Elemental annual mean % are calculated using the annual mean
920 emission of each element divided by the annual mean emission of dust.

921 Fig.9 Ten year averaged Ca/Al ratio in (a) dust emission of source regions and (b) dust deposition into various ocean
922 basins and glaciers. Elemental ratios are calculated using the annual mean emission of Ca divided by the annual
923 mean emission of Al.

924 Fig.10 Comparison of observed and modeled mean fractions of elements at each site for (a) total
925 suspended particulates (TSP) and (b) PM_{2.5}. (1-Hetian, China; 2-Tazhong, China; 3-Yu Lin, China; 4-
926 Duolun, China; 5-Shengsi, China; 6-Hanoi, Vietnam; 7-Marnila, Philippines; 8-Balad, Iraq; 9-Baghdad,
927 Iraq; 10-Taji,Iraq; 11-Eilat; 12-Cape Verde Island; 13-Muswellbrook, Australia; 14-Richmond,
928 Australia, 15-Tamanrasset, Algeria; 16-Banizoumbou, Niger; 17-Douz, Tunisia). Here we calculate the
929 elemental fractions and average the fractions temporally for each site and compare to observations.
930

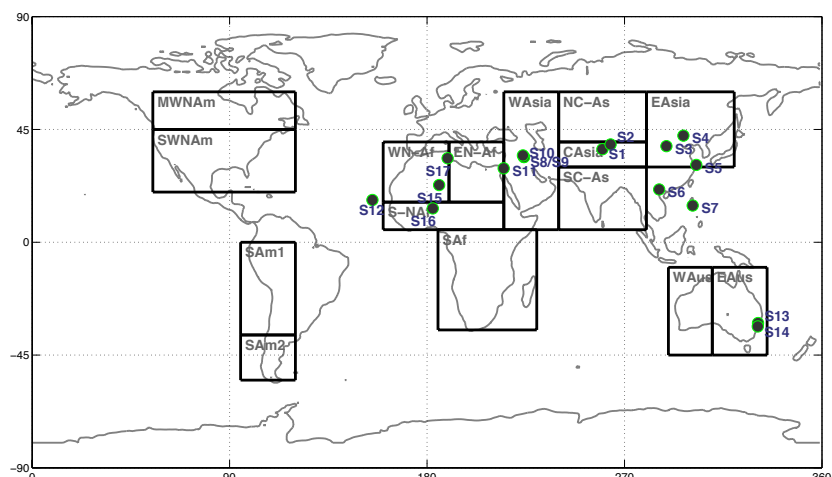
931 Fig.11 Mean and quartile modeled and observational fractions of elements in (a) TSP (b) PM_{2.5} for all
932 sites together, the box line presents 25%, 50% and 75%, individually. Here we calculate the elemental
933 fractions and average the fractions temporally for each site and compare to observations.
934

935 Fig.12 (a) Observational and (b) modeled dust deposition (g/m³/year). The scale is the same for both
936 panels. (c) A scatterplot shows the comparison between the model and observations. The correlation
937 coefficient between observations and model results reach 0.86.

938 Fig.13 Percentages of elements in dust deposition (%) after tuning. It is tuned based on original
939 percentages of elements in dust deposition in Fig. S1 by timing Obs./Mod. ratios listed in Table 3. Si
940 did not change because there are not enough observational data available

941 Fig. 14 Fractional solubility of elements (soluble element / total element) in dust deposition (%):a. Mg, b.
942 P, c. Ca, d. Mn, e. Fe, f. K, g. Al, h. Si

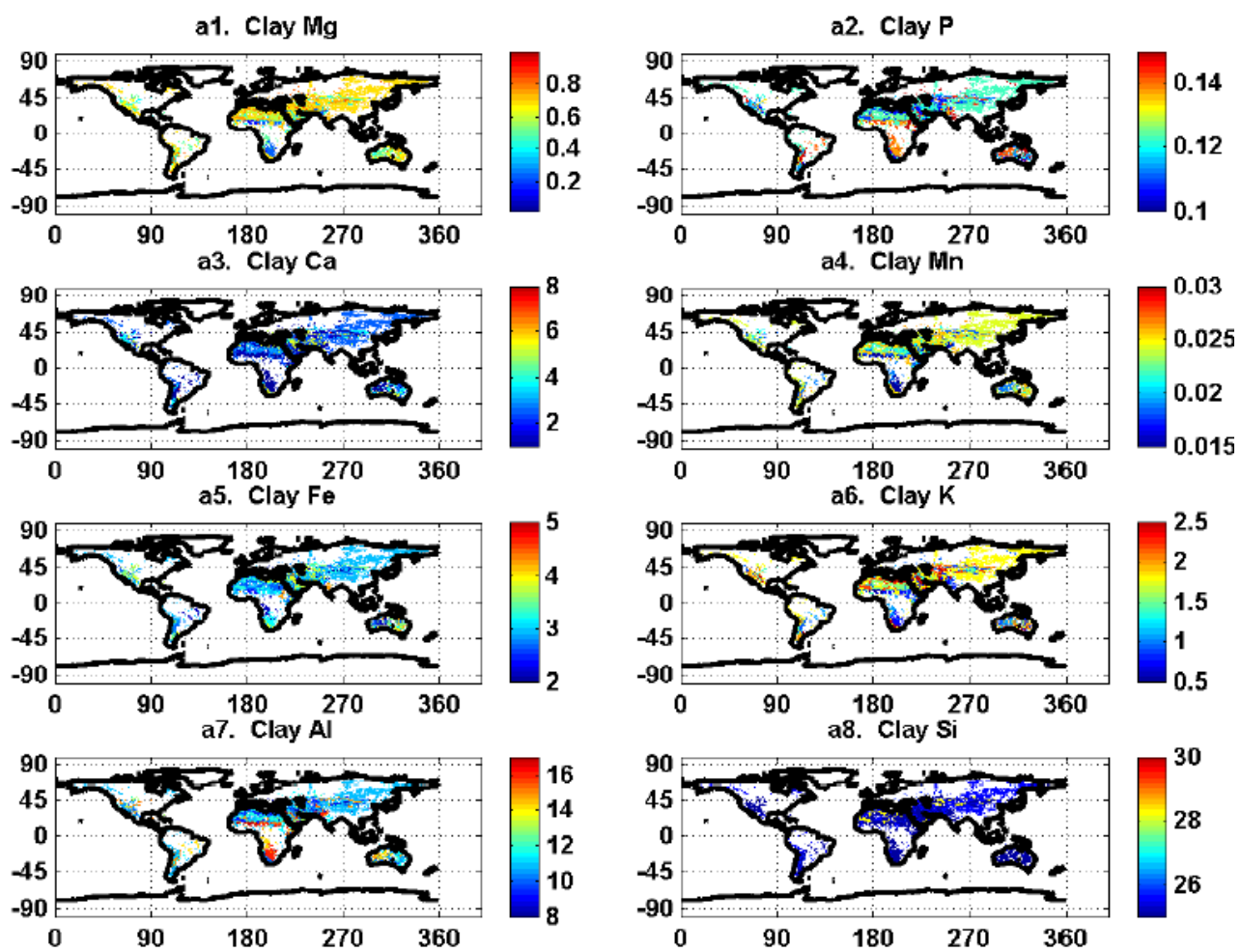
943 Fig. 15 Percentages of soluble elements in total dust deposition using (a) Sol-1 & (b) Sol-2 (‰), Sol-1
944 refer to mineral method after tuning, Sol-2 refer to Sillanpaa method described in the methods section
945 (2).



946

947 **Fig.1. Observational sites** (S1-Hetian, China; S2-Tazhong, China; S3-Yu Lin, China; S4-Duolun,
 948 China; S5-Shengsi, China; S6-Hanoi, Vietnam; S7-Marnila, Philippines; S8- Balad, Iraq; S9-Balad,
 949 Iraq; S10-Taji, Iraq; S11-Eilat; S12-Cape Verde Atmospheric Observatory (CVAO); S13-
 950 Muswellbrook, Australia; S14-Richmond, Australia; S15-Tamanrasset, Algeria; S16-Banizoumbou,
 951 Niger; S17-Douz, Tunisia) **and dust-producing regions** (WASia: West Asia; NC-As: North Central
 952 Asia; CAsia: Central Asia; SC-As: South Central Asia; EAsia:East Asia; WN-Af:North West Africa;
 953 EN-Af: North East Africa; S-NAf: Southern North Africa; SAf: Southern Africa; MWNAm: Middle
 954 North West America; SWNAm: Southern North West America; SAM1: Northern South America;
 955 SAM2: Southern South America; WAus: West Australia; EAus: East Australia)

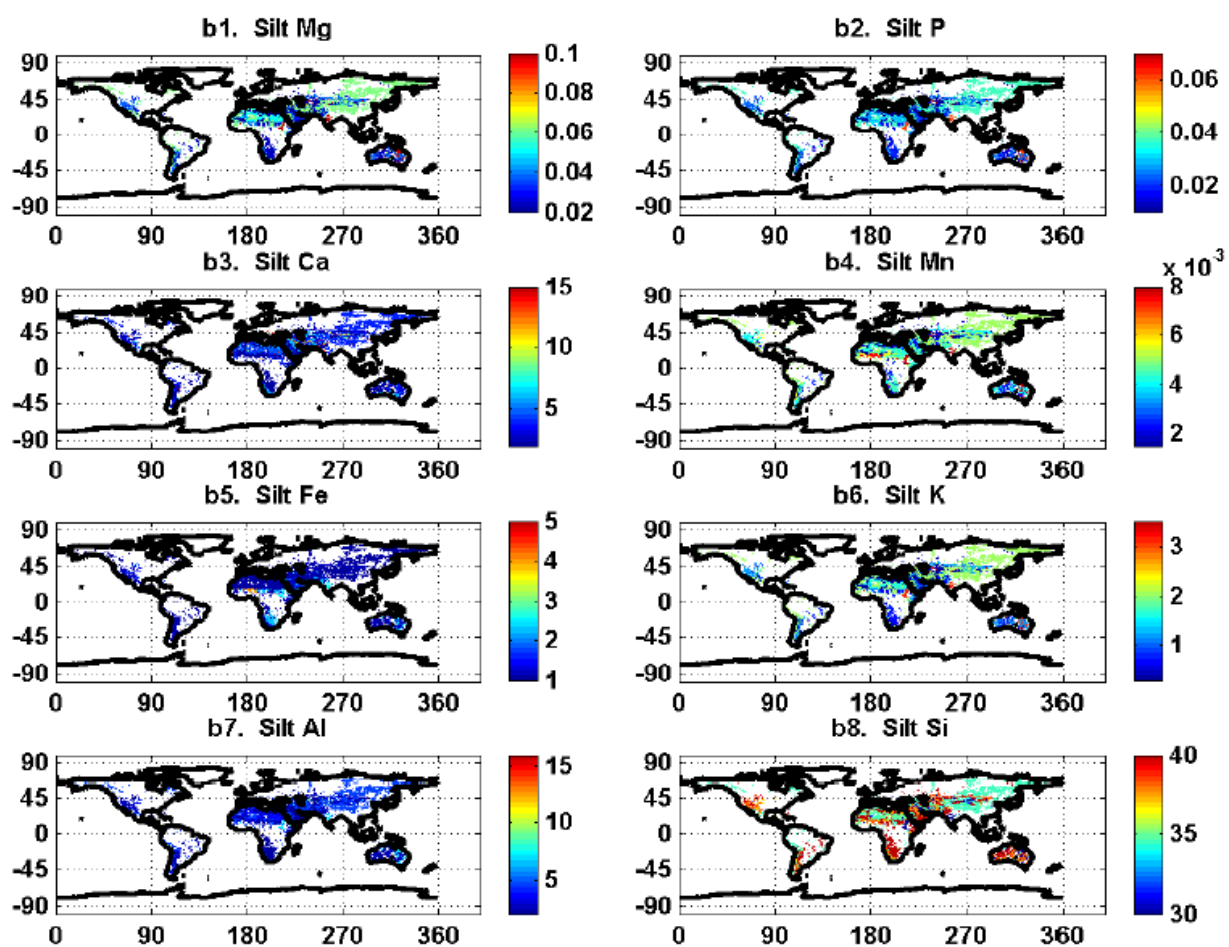
956



957

958

(a) in soil clay



959

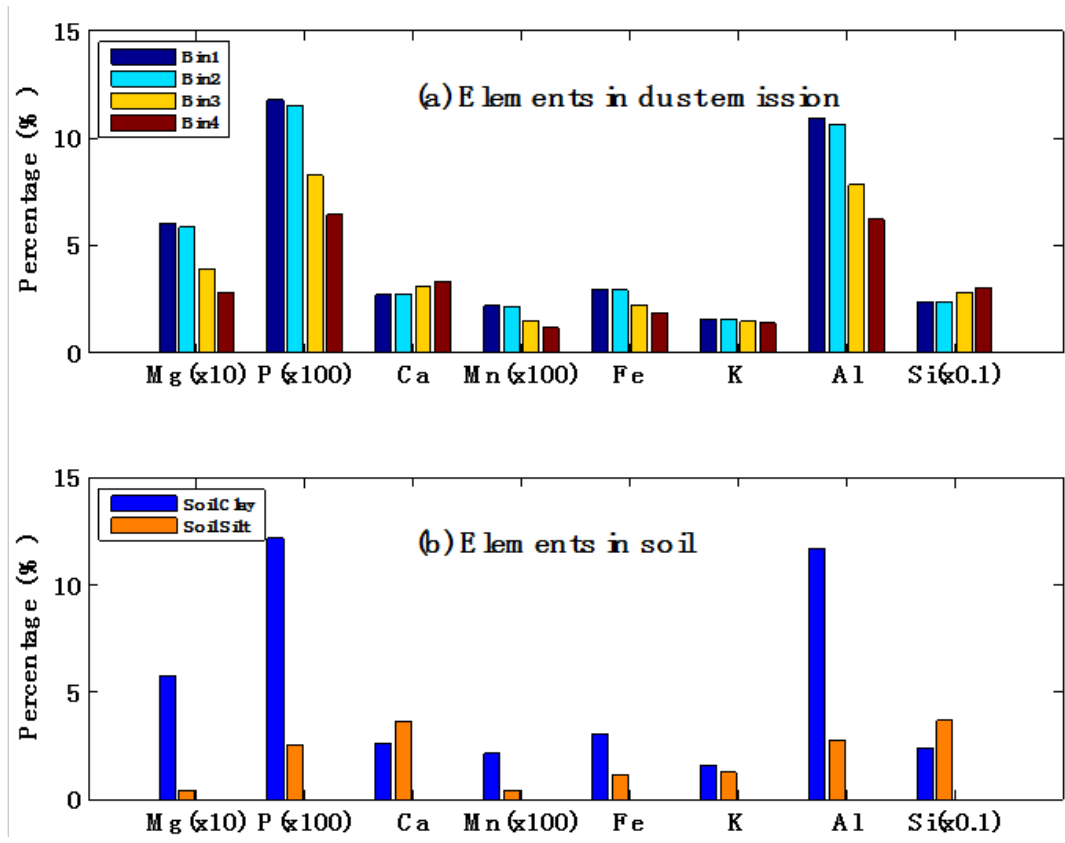
960

(b) in soil silt

961 Fig.2 Global elemental distributions (in mass percentage) in (a) soil clay, a1: Clay Mg, a2: Clay P, a3: Clay Ca, a4:

962 Clay Mn, a5: Clay Fe, a6: Clay K, a7: Clay Al, a8: Clay Si; (b) soil silt, b1: Silt Mg, b2: Silt P, b3: Silt Ca, b4:

963 Silt Mn, b5: Silt Fe, b6: Silt K, b7: Silt Al, b8: Silt Si.

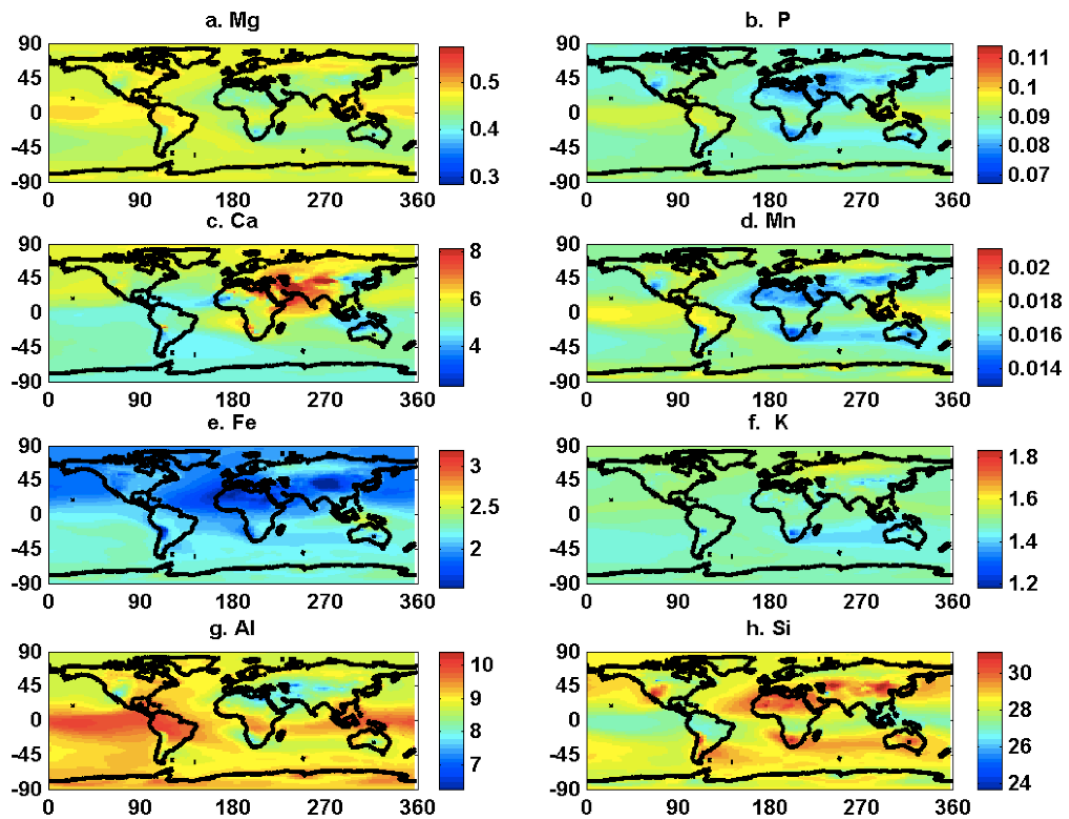


964

965 Fig.3 Global mean elemental percentages in (a) four-bin dust emission and (b) clay and silt fractions of soils (Bin1-4
 966 refer to particle range listed in Table S2, clay refer to < 2 μ m, silt refer to > 2 μ m)

967

968



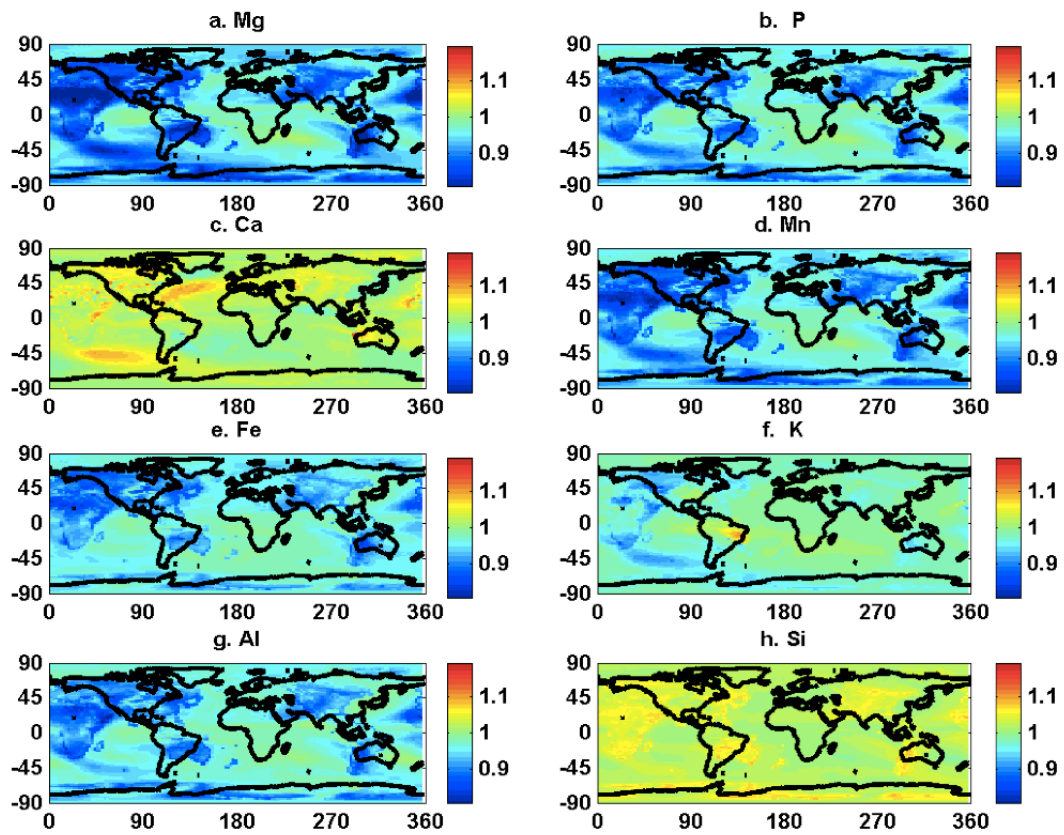
969

970 Fig.4 Percentages of elements in dust concentration (mass %) : a. Mg, b. P, c. Ca, d. Mn, e. Fe, f. K, g. Al, h. Si.

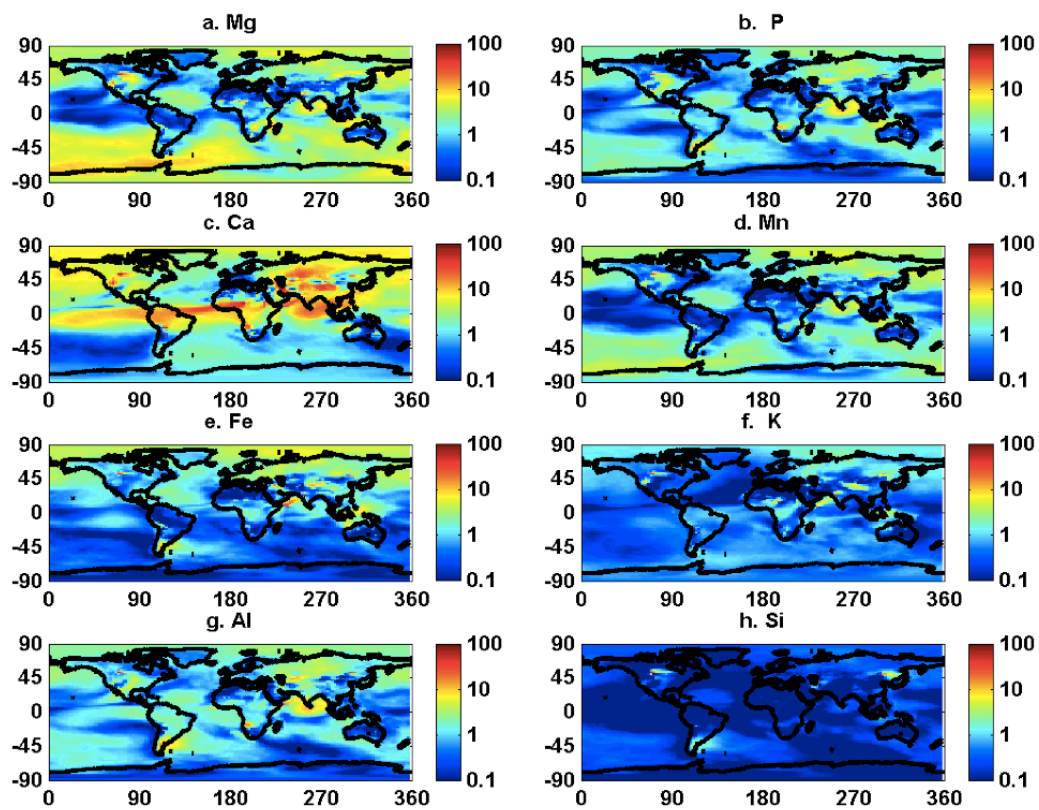
971 Elemental % shown here are calculated using the annual mean element concentration divided by the annual mean

972 dust concentration.

973



976 Fig.5 Ratio of mass fractions of elements in dust deposition to that in atmospheric dust : a. Mg, b. P, c. Ca, d. Mn, e.
 977 Fe, f. K, g. Al, h. Si. Elemental ratios shown here are calculated using the annual mean element deposition divided
 978 by the annual mean dust deposition.



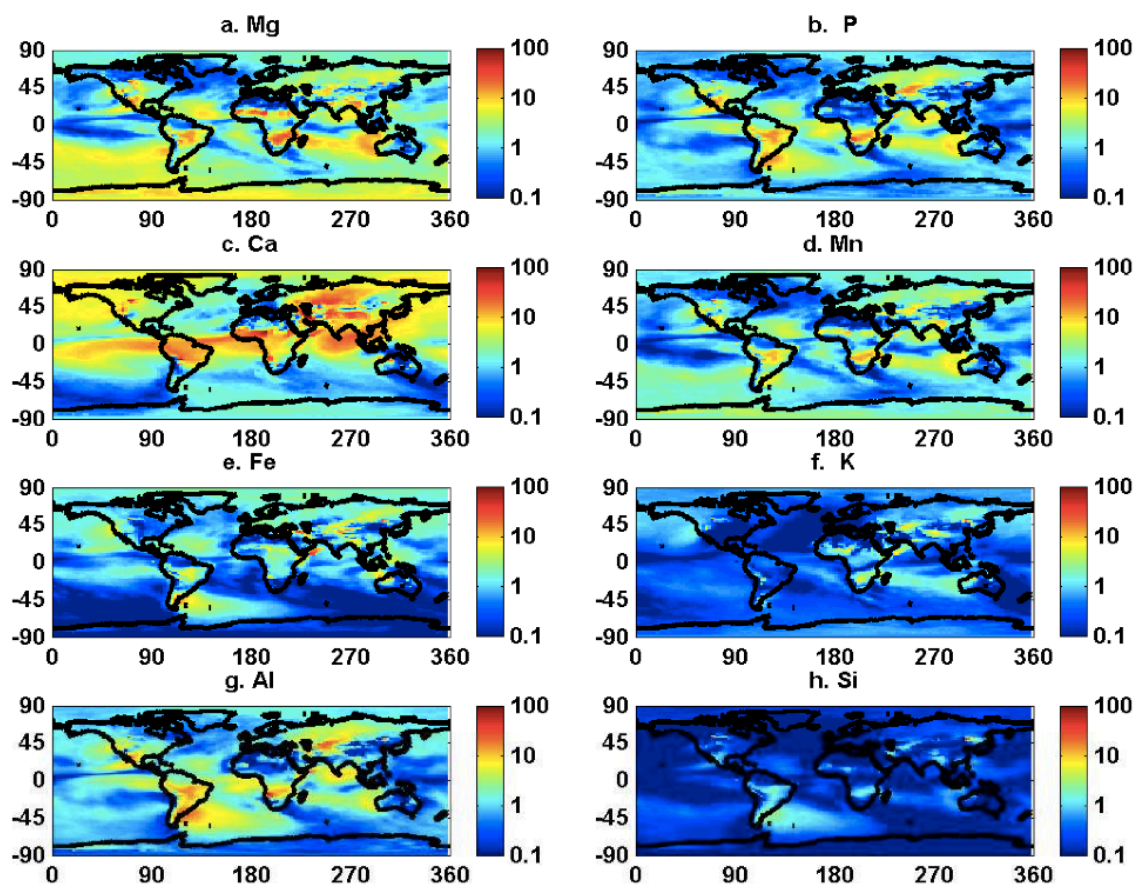
979

980 Fig.6 Ten-year monthly variability in mean of elemental percentages in atmospheric dust (mass %) : a. Mg, b. P, c.

981 Ca, d. Mn, e. Fe, f. K, g. Al, h. Si. Elemental monthly mean % are calculated using the monthly mean emission of

982 each element divided by the monthly mean emission of dust.

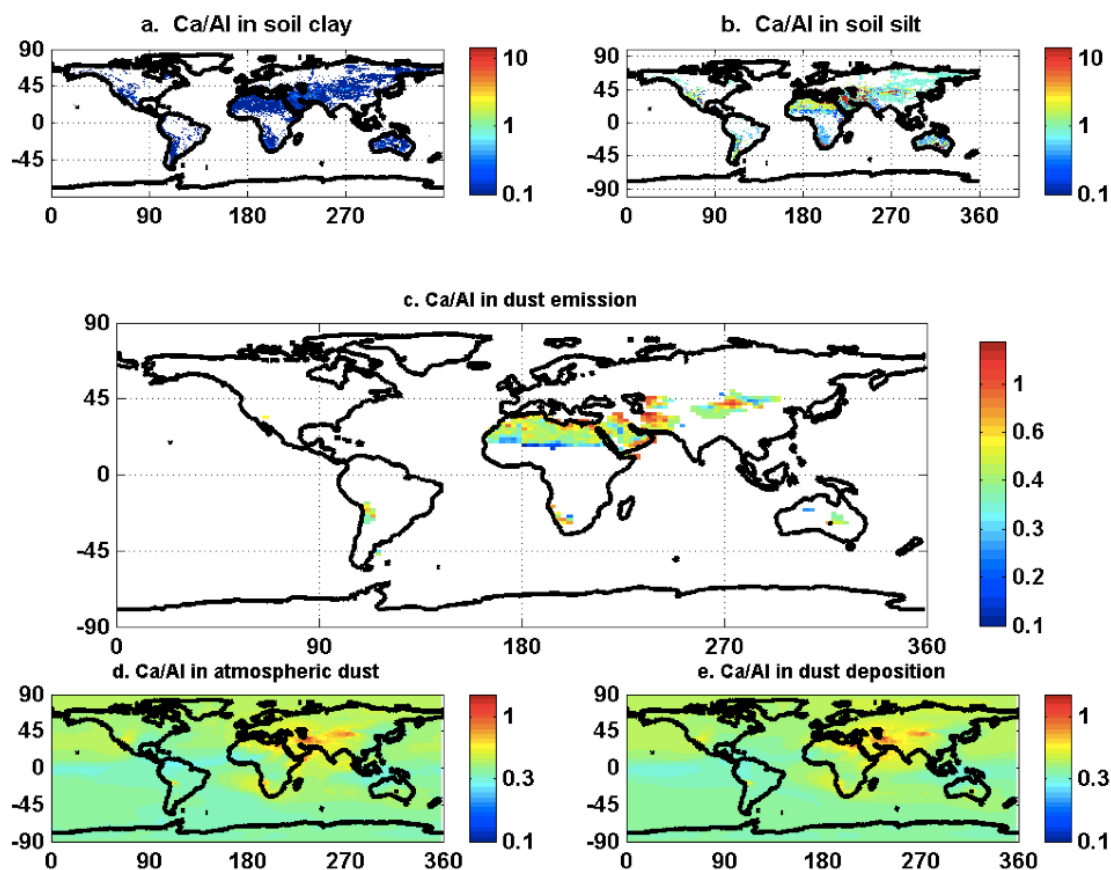
983



984

985 Fig.7 Ten-year monthly variability in mean of elemental percentages in dust deposition (mass %):a. Mg, b. P, c. Ca,
 986 d. Mn, e. Fe, f. K, g. Al, h. Si. Elemental monthly mean % are calculated using the monthly mean emission of each
 987 element divided by the monthly mean emission of dust.

988

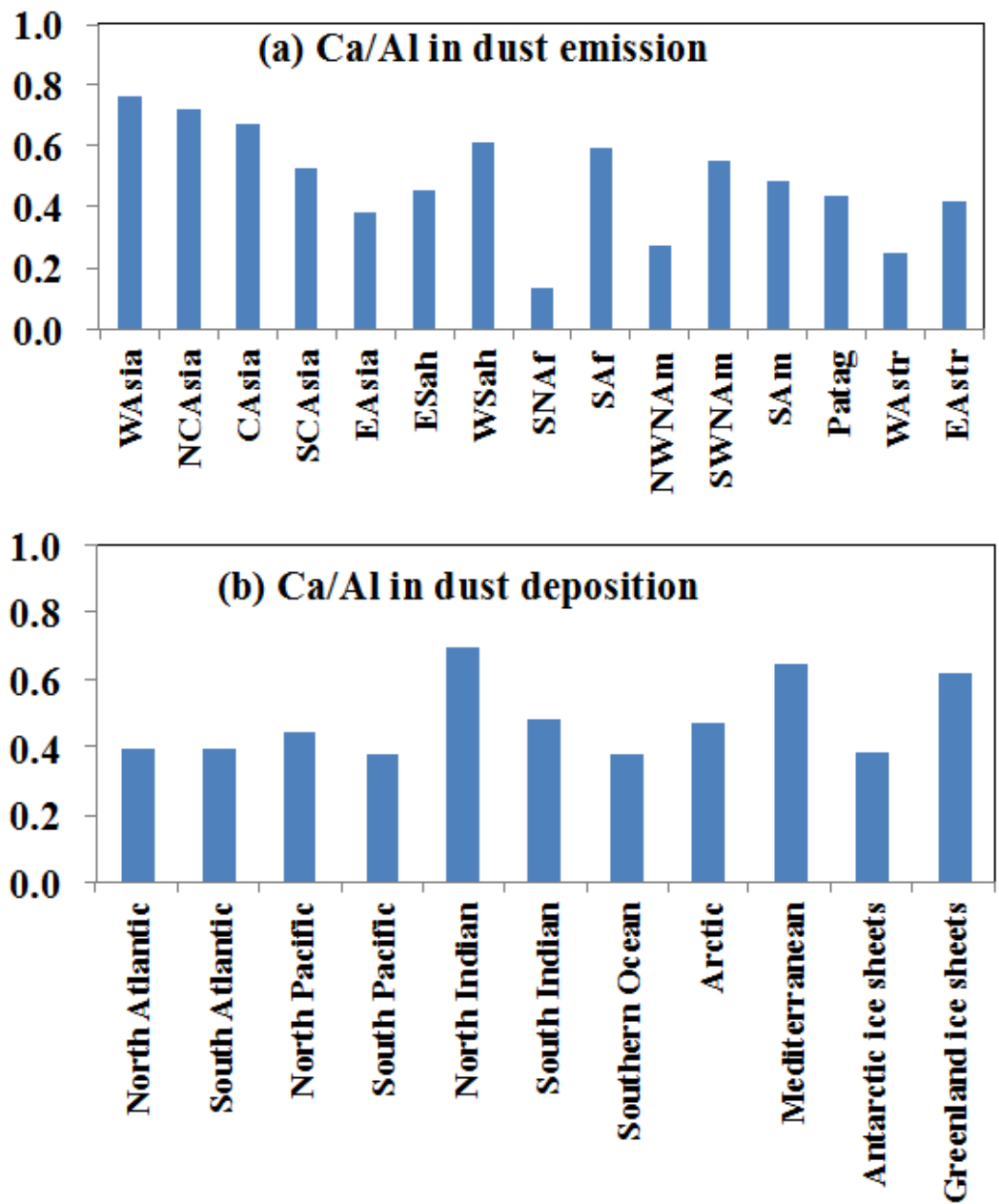


989

990

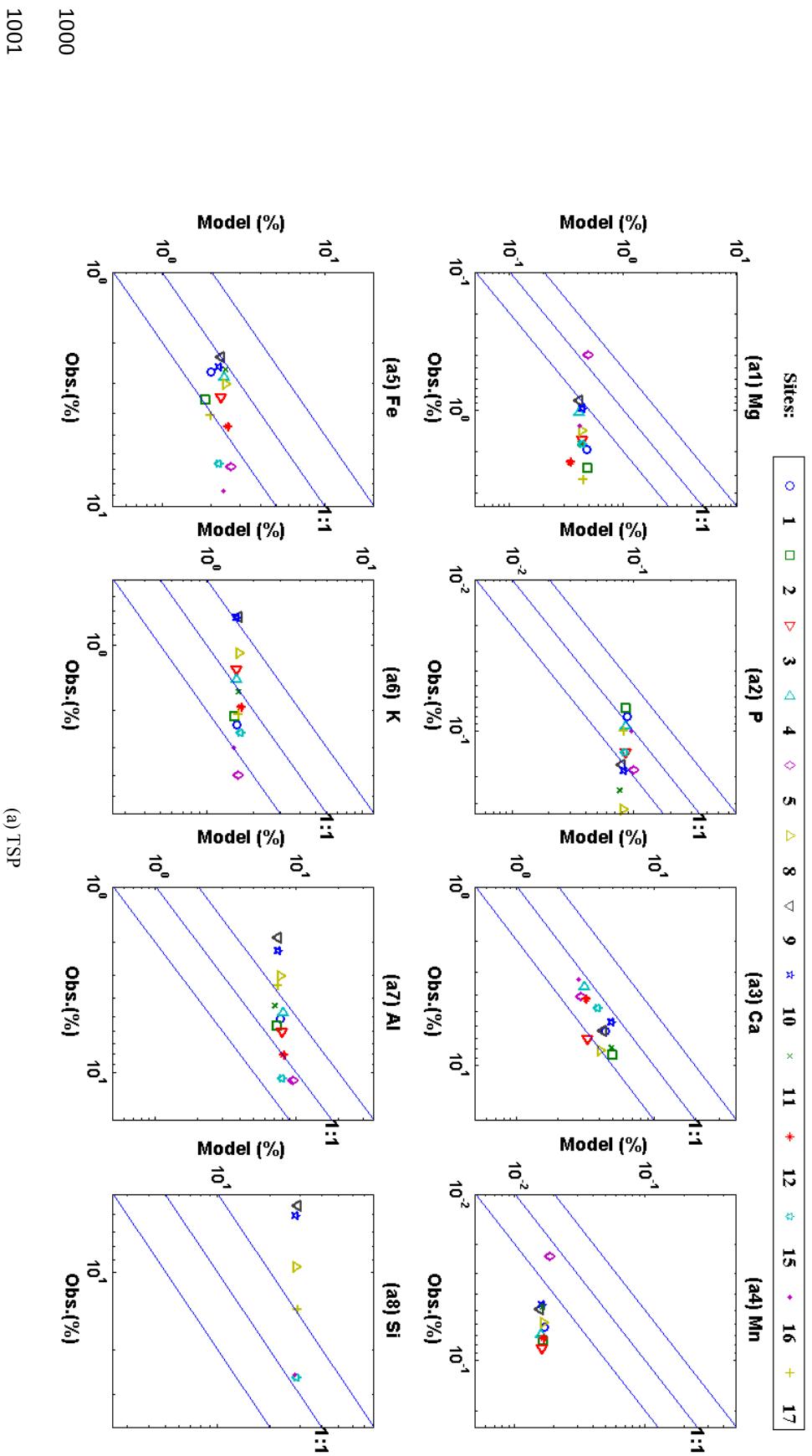
991 Fig.8 Ca/Al in Soil and ten year averaged Ca/Al ratio in dust emission, concentration and deposition. Top two (a,b)
 992 refer to ratio in clay and silt desert soil, middle one (c) refer to ratio in dust emission, and bottom two (d,e) refer to
 993 ratio in dust concentration and deposition. Elemental annual mean % are calculated using the annual mean
 994 emission of each element divided by the annual mean emission of dust.

995



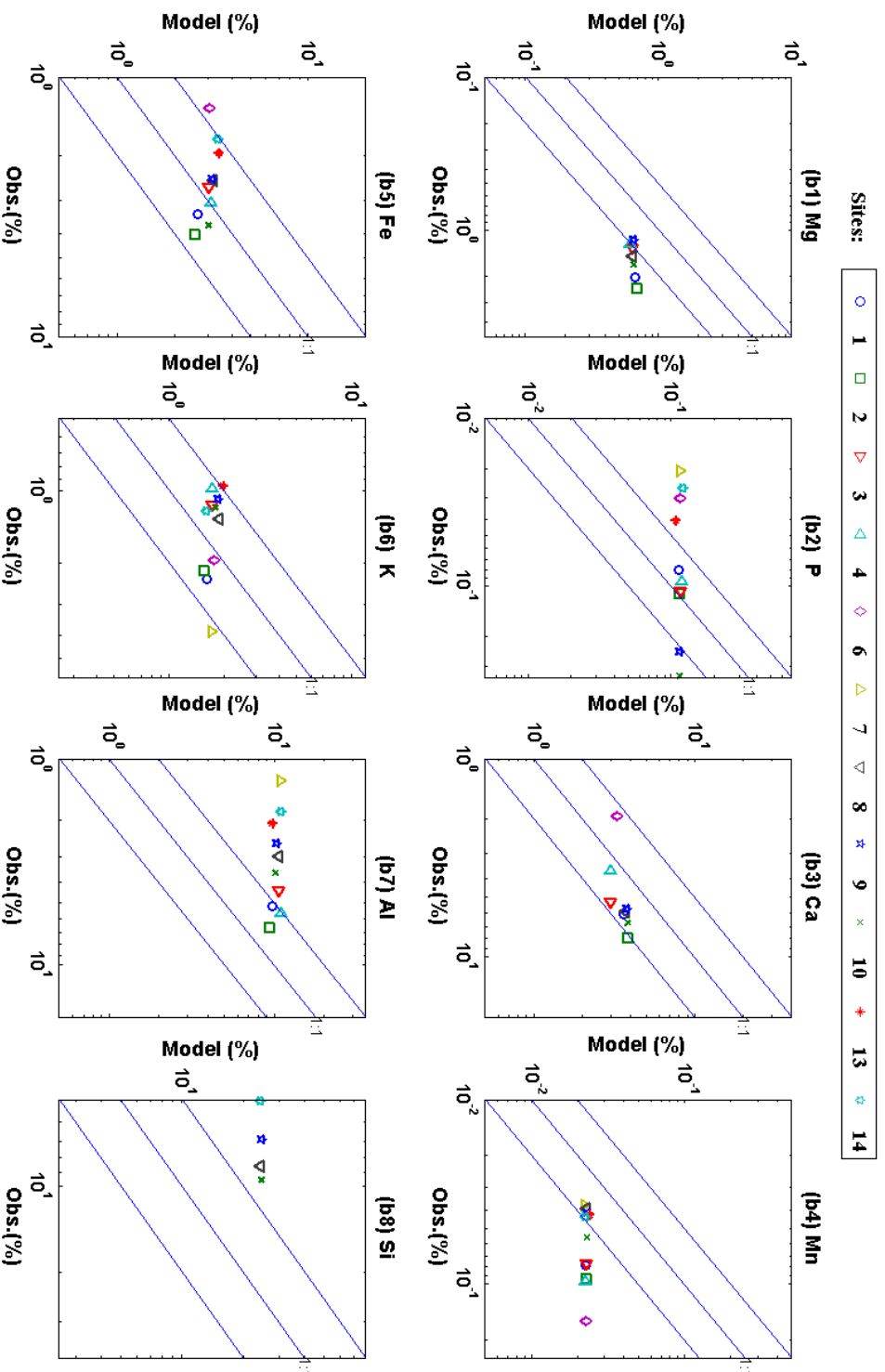
996

997 Fig.9 Ten year averaged Ca/Al ratio in (a) dust emission of source regions and (b) dust deposition into various ocean
 998 basins and glaciers. Elemental ratios are calculated using the annual mean emission of Ca divided by the annual
 999 mean emission of Al.



1000

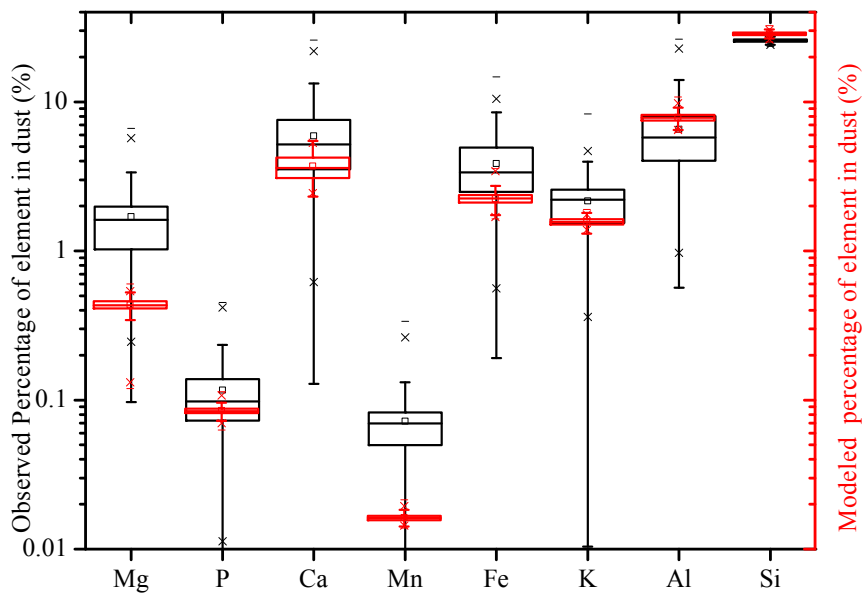
1001



(b) $PM_{2.5}$

1003 Fig.10 Comparison of observed and modeled mean fractions of elements at each site for (a) total suspended particulates (TSP) and (b) $PM_{2.5}$: (1-Hetian, China; 2-Tazhong,
 1004 China; 3-Yu Lin, China; 4-Duolun, China; 5-Shengsi, China; 6-Hanoi, Vietnam; 7-Marrila, Philippines; 8-Balad, Iraq; 9-Baghdad, Iraq; 10-Taji, Iraq; 11-Eilat; 12-Cape Verde
 1005 Island; 13-Muswellbrook, Australia; 14-Richmond, Australia; 15-Tamanrasset, Algeria; 16-Banzoumbou, Niger; 17-Douz, Tunisia). Here we calculate the elemental fractions
 1006 and average the fractions temporally for each site and compare to observations.
 1007

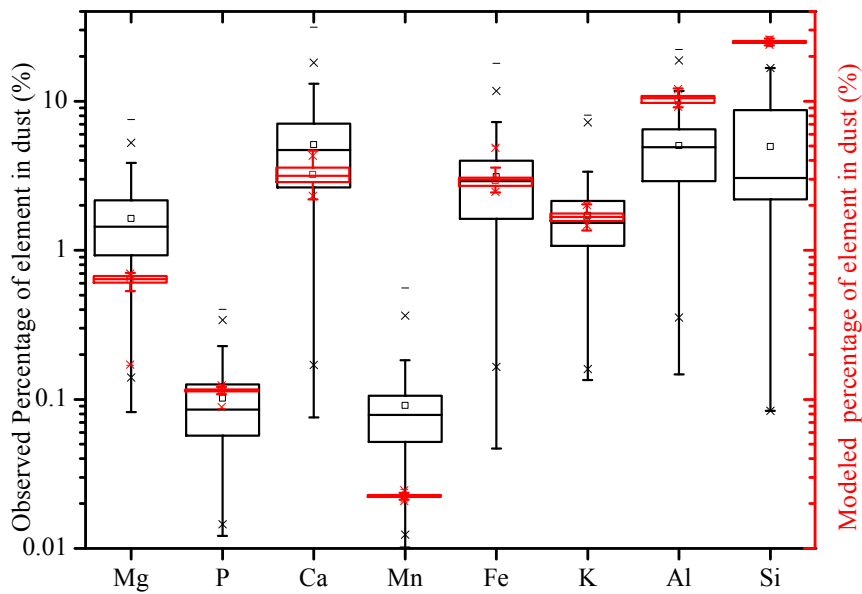
1008



1009

1010

(a) TSP

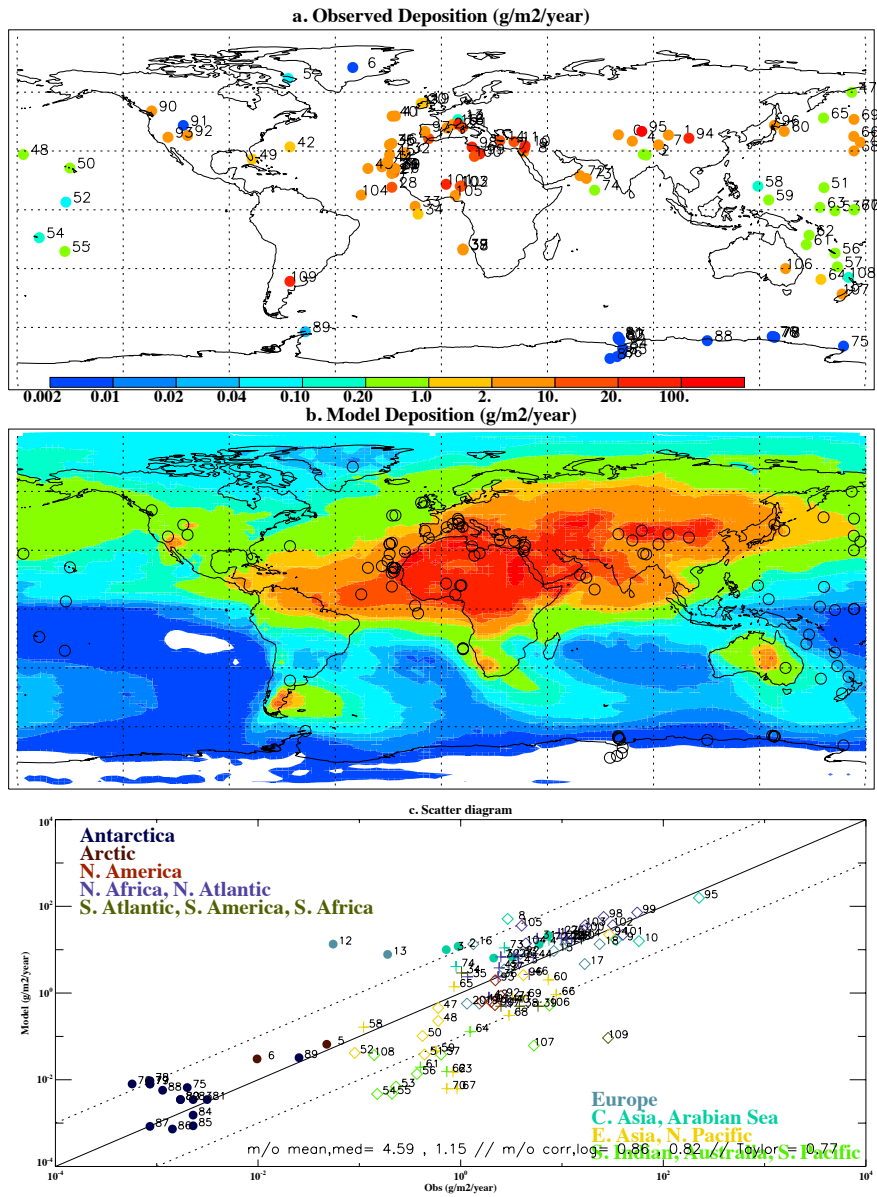


1011

1012

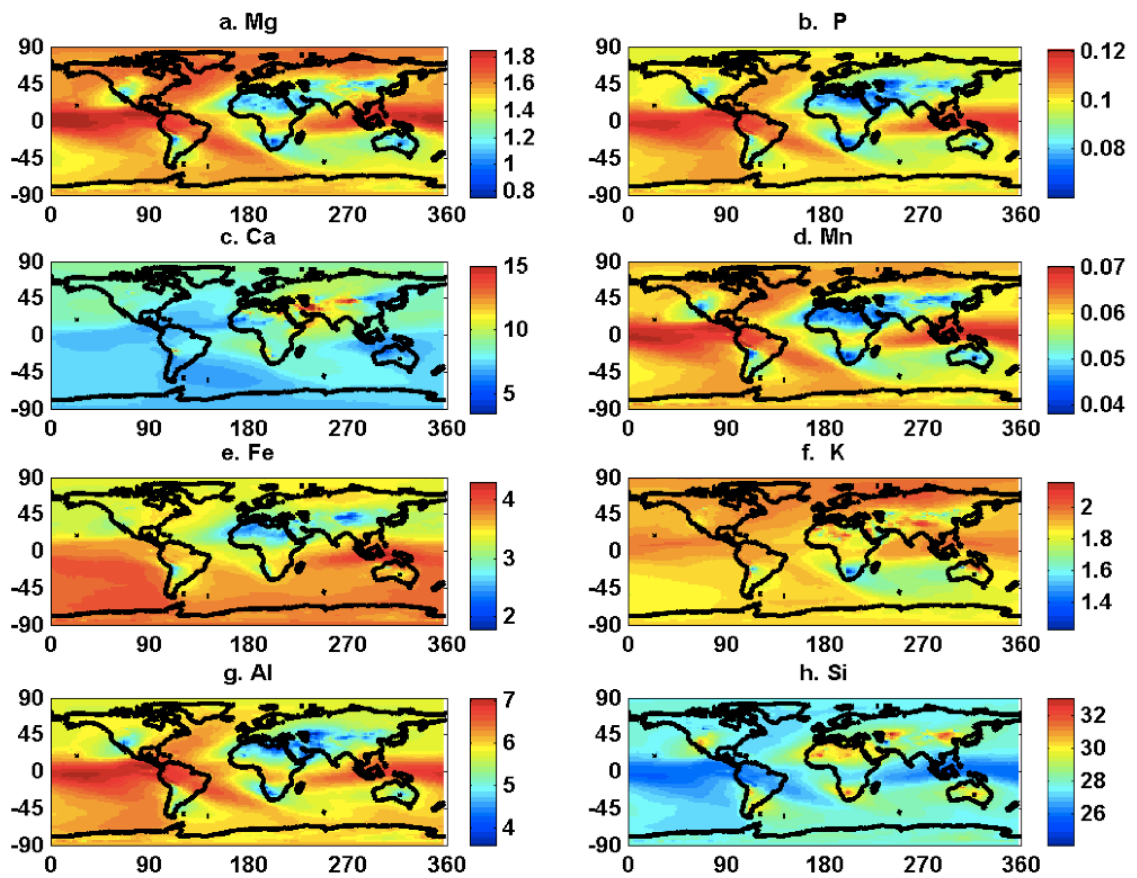
(b) PM_{2.5}

1013 Fig.11 Mean and quartile modeled and observational fractions of elements in (a) TSP (b) PM_{2.5} for all
1014 sites together, the box line presents 25%, 50% and 75%, individually. Here we calculate the elemental
1015 fractions and average the fractions temporally for each site and compare to observations.



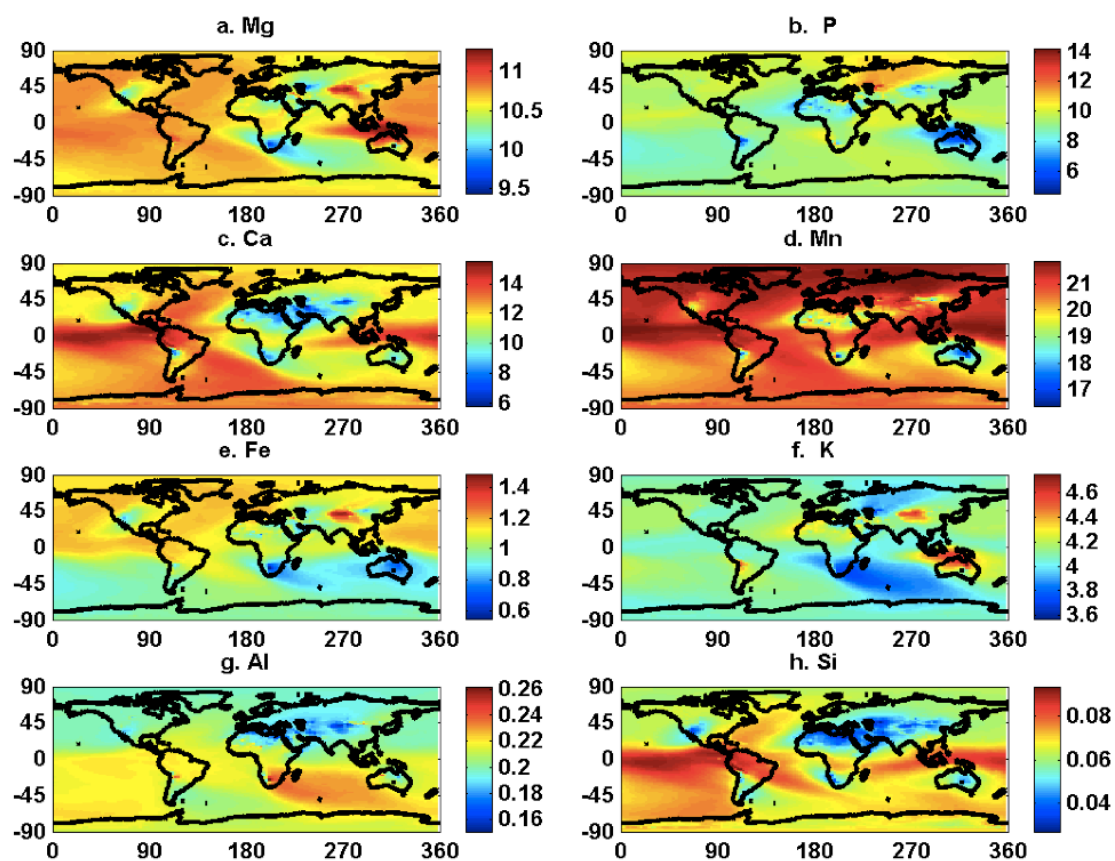
1016

1017 Fig.12 (a) Observational and (b) modeled dust deposition (g/m³/year). The scale is the same for both
 1018 panels. (c) A scatterplot shows the comparison between the model and observations. The correlation
 1019 coefficient between observations and model results reach 0.86.



1020

1021 Fig.13 Percentages of elements in dust deposition (%) after tuning. It is tuned based on original
 1022 percentages of elements in dust deposition in Fig. S1 by timing Obs./Mod. ratios listed in Table 3. Si
 1023 did not change because there are not enough observational data available



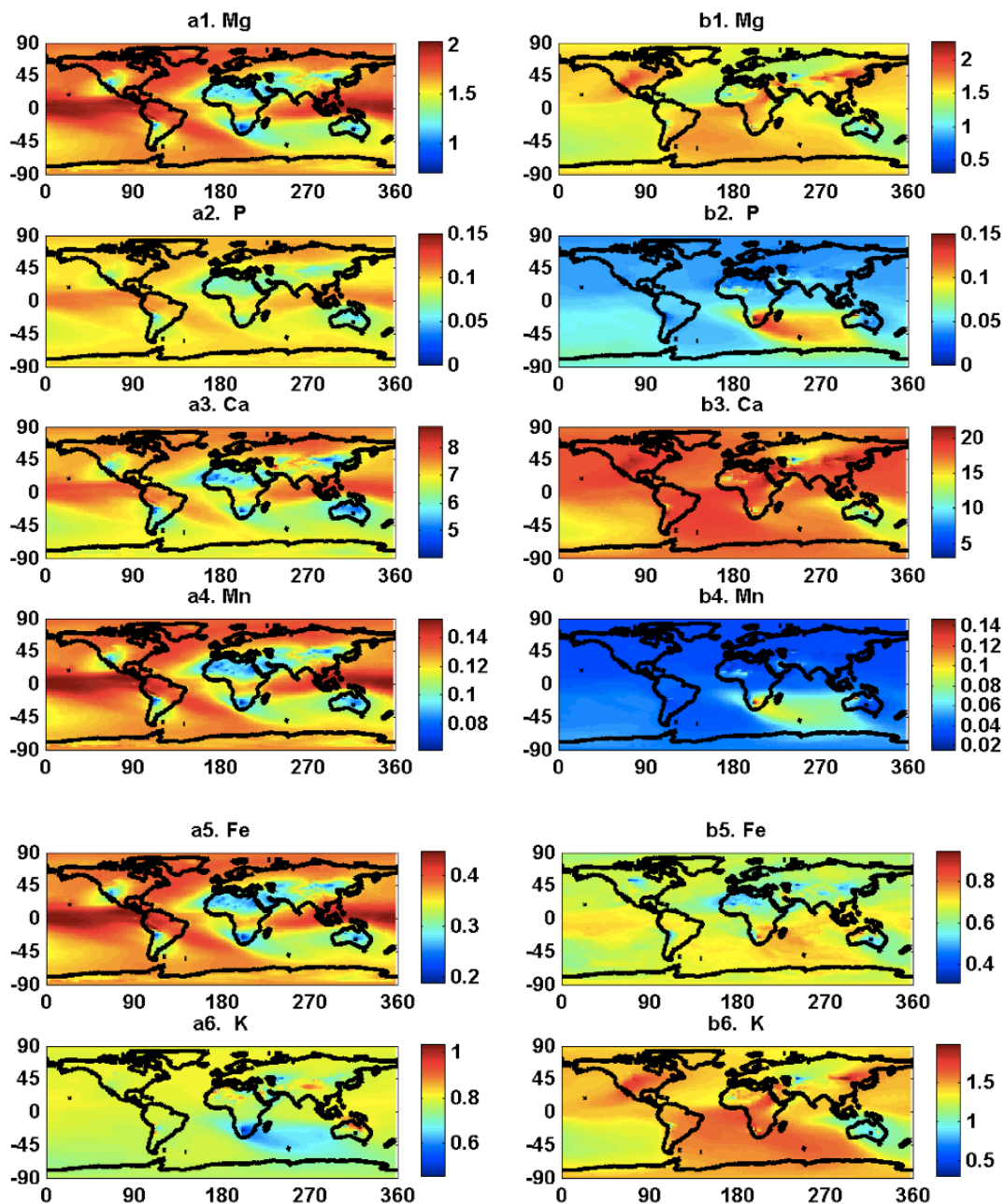
1024

1025 Fig. 14 Fractional solubility of elements (soluble element / total element) in dust deposition (%):a. Mg, b.

1026 P, c. Ca, d. Mn, e. Fe, f. K, g. Al, h. Si

1027

1028



1029

1030

1031 Fig. 15 Percentages of soluble elements in total dust deposition using (a) Sol-1 & (b) Sol-2 (%), Sol-1
1032 refer to mineral method after tuning, Sol-2 refer to Sillanpaa method described in the methods section
1033 (2).

1034

1035